AGU100 ADVANCING EARTH AND SPACE SCIENCE

Tectonics

RESEARCH ARTICLE
10.1029/2018TC004984

Key Points:
- Meteoric, not magmatic, fluids interacted with the low-angle Mormon Peak and Heart Mountain detachments
- Clumped-isotope thermometry can record a frictional heating signal, but it is rare on the Mormon Peak detachment and absent on the main Heart Mountain detachment
- Most fault breccias, gouges, and clastic dikes preserve temperatures that are colder than the host rock

Supporting Information:
- Supporting Information S1
- Table S1

Correspondence to:
E. M. Swanson,
eswanson@caltech.edu;
emswanson@lanl.gov

Citation:
Swanson, E. M., Wernicke, B. P., & Eiler, J. M. (2018). Fluid flow, brecciation, and shear heating on faults: Insights from carbonate clumped-isotope thermometry. *Tectonics*, *37*, 2938–2960. https://doi.org/10.1029/2018TC004984

Received 7 FEB 2018
Accepted 4 AUG 2018
Accepted article online 17 AUG 2018
Published online 8 SEP 2018

Fluid Flow, Brecciation, and Shear Heating on Faults: Insights From Carbonate Clumped-Isotope Thermometry

E. M. Swanson[1,2], B. P. Wernicke[1], and J. M. Eiler[1]

[1]Division of Geological and Planetary Sciences, California Institute of Technology, Pasadena, CA, USA, [2]Now at Los Alamos National Laboratory, Los Alamos, NM, USA

Abstract Slip on gently dipping detachments in the brittle crust has been enigmatic for decades, because fracture mechanics laws predict frictional resistance is too great for sliding to occur, except under rather unusual circumstances. The Miocene Mormon Peak detachment in Nevada and the Eocene Heart Mountain detachment in Wyoming are two well-studied examples of upper crustal, carbonate-hosted low-angle detachments, with highly debated slip processes. Both low-angle faults were active during regional magmatism, and a number of proposed slip mechanisms involve magmatic fluids, frictional heating, or both. To address the role that magmatic fluids and frictional heating may have played in reducing friction, we measured clumped-isotope ratios on 137 carbonate samples from these faults. The majority of fault breccias and gouges on the detachment slip surface record temperatures that are colder than the host rock. Surprisingly, samples from within 5 m of the Heart Mountain detachment average just 65 °C, and not a single sample (out of 37 measurements, excluding metamorphosed host rock at White Mountain) records a temperature greater than 90 °C. Along both faults, most samples are depleted in $\delta^{18}O$ relative to the host rock, indicating that meteoric, not magmatic, fluids were present and interacting with the fault rock. However, a few samples preserve temperatures of over 160 °C, which, based on textural and geochemical criteria, are difficult to explain other than by frictional heating during slip. These temperatures are recorded in one sample directly on the Mormon Peak detachment slip surface and in two hanging wall localities above the Heart Mountain detachment.

Plain Language Summary Some faults are oriented such that friction should prevent them from sliding, but show evidence of slip. Some of the potential explanations involve weakening processes that occur from heating on the fault, either from friction or from magmatic fluids. Here we use carbonate clumped-isotope thermometry to look for heating signals preserved in the rock and use the carbon and oxygen isotopes to determine the source of the heat. We find that most of the rocks preserve a surprisingly cold temperature, while a small number do preserve a heating event that we interpret to be from friction.

1. Introduction

The classic Andersonian theory of fault mechanics presumes that the Earth obeys Coulombic failure criteria and that one of the principal stress axes is normal to the Earth's surface. Under these conditions, the ratio of shear stress to normal stress on low-angle normal faults (<30°) is too low for either fracture initiation or slip on a preexisting fracture, even if the ambient pore fluid pressure is lithostatic (e.g., Axen, 2004). The ubiquity of normal faults that both formed and slipped at low angle (e.g., Lister & Davis, 1989; Livaccari & Geissman, 2001; Morley, 2014; Mount & Suppe, 1987; Pierce, 1980; Scott & Lister, 1992; Wernicke, 1995) has accordingly led to extensive theoretical, experimental, and field research into this enduring enigma, resulting in explanations that emphasize some form of fluid-assisted weakening of fault zone materials, rotation of stress axes, or both (e.g., Axen, 1992; Bos & Spiers, 2001; Collettini & Holdsworth, 2004; Forsyth, 1992; Lister & Baldwin, 1993; Melosh, 1990; Parsons & Thompson, 1993; Yin, 1989; Zoback & Townend, 2001). The same puzzle arises in the case of major strike-slip faults such as the San Andreas, which also appears to be oriented nearly perpendicular to the maximum principal stress direction in the upper crust (e.g., Hickman & Zoback, 2004; Lockner et al., 2011; Mount & Suppe, 1987; Rice, 1992). It is therefore generally acknowledged that the lack of resolution of this "stress paradox" remains the primary hurdle in understanding the mechanics of faulting.

Fluid-assisted weakening mechanisms generally invoke high temperatures, due to (1) friction, up to and including melting in silicate rocks (e.g., Cowan, 1999; Hirose & Shimamoto, 2005; Sibson, 1975), or

decarbonation in carbonate rocks (e.g., Han et al., 2010; Sulem & Famin, 2009), or (2) magmatism, including the injection of volcanic gases (Hughes, 1970) and pressurization via magmatic heating of pore waters (Aharonov & Anders, 2006). Weakening may thus occur by reducing the coefficient of friction (as appears to be the case for the San Andreas fault at shallow depth; Lockner et al., 2011) or by the development of near-lithostatic overpressure confined to the slip zone (e.g., DePaola et al., 2011; Rice, 2006).

In this paper, we investigate the extent to which these mechanisms might apply to natural faults by using carbonate clumped-isotope thermometry on fault rocks and veins to track the origin and thermal evolution of fault zone fluids. In order to apply this technique to fault systems, we have focused on two carbonate-hosted, upper crustal low-angle faults, including the Heart Mountain detachment in the Absaroka Range and environs in NW Wyoming and the Mormon Peak detachment in the Mormon Mountains in SE Nevada. Both faults are well exposed over areas of c. 1,000 km^2 and have displacements of at least 10 km. Because both faults primarily involve lower Paleozoic dolomitic strata in platform margin or cratonic settings, their stable isotope composition is quite heavy in both oxygen ($\delta^{18}O$ c. +20–25‰ Vienna Standard Mean Ocean Water, VSMOW) and carbon ($\delta^{13}C$ c. 0–4‰ Vienna Pee Dee Belemnite, VPDB), so that exchange phenomena with relatively light meteoric water and magmatic fluids can be expected to yield robust signals. Accordingly, each of the two areas has an extensive history of investigation both structurally and isotopically (for Heart Mountain: Anders et al., 2010; Douglas et al., 2003; Hauge, 1985, 1990; Pierce, 1980; Templeton et al., 1995; and for the Mormon Mountains: Anders et al., 2006; Anderson et al., 2010; Axen et al., 1990; Diehl et al., 2010; Losh, 1997; Swanson et al., 2012; Walker et al., 2007; Wernicke et al., 1985). Our purpose here is to add a perspective from clumped-isotope geochemistry on these two well-characterized damage zones. Both the Heart Mountain and Mormon Peak detachments developed synchronously with regional magmatism, the former during development of the Eocene Absaroka Volcanic Supergroup (c. 52–48 Ma; Feeley & Cosca, 2003; Smedes & Prostka, 1972) and the latter during the development of the Miocene Kane Springs Wash caldera (c. 15–14 Ma; Scott et al., 1995).

The faults exhibit two key distinctions in their mode of origin that bear on the interpretation of thermometric data, including (1) their proximity to coeval magmatic centers and (2) their depth of development. The Heart Mountain detachment and allochthon are generally regarded as resulting from the gravitational collapse of a sector of a magmatic center (Sunlight Volcano and related units), with the detachment initiating at a depth of 1,000–2,000 m (Beutner & Hauge, 2009, and references therein). In contrast, the Mormon Peak detachment and allochthon developed more distant from magmatism, about 30–40 km SE of the Kane Springs Wash caldera. The detachment is a normal fault that has exhumed structural depths in its footwall that are in excess of 6,000 m (Axen et al., 1990; Bidgoli et al., 2015; Swanson et al., 2012; Swanson & Wernicke, 2017). Thus, these two faults provide excellent opportunities to look for evidence of heating processes that might facilitate slip along low-angle slip surfaces and distinguish whether frictional heating and/or magmatic heating was involved.

2. Carbonate Clumped-Isotope Thermometry

Carbonate clumped-isotope thermometry is a relatively new technique for measuring the temperature of carbonate mineral crystallization. The bonding of the heavy isotopes ^{13}C and ^{18}O to each other is a temperature-dependent process and is measurable with current mass spectrometry techniques (Eiler, 2007). This effect can be described as an exchange reaction with the form

$$Ca^{13}C^{16}O_3 + Ca^{12}C^{18}O^{16}O_2 = Ca^{13}C^{18}O^{16}O_2 + Ca^{12}C^{16}O_3$$

The forward reaction causes "clumping" of the more massive ^{13}C and ^{18}O isotopes. The extent to which this forward reaction is favored depends on the balance between the lower vibrational energy of the ^{13}C-^{18}O bond and the entropy of the system, as described in Schauble et al. (2006). At higher temperatures, a more random distribution is favored, whereas at lower temperatures, clumping is preferred. This degree of ordering is set during crystallization at temperatures less than ~200 to 300 °C but can be readily modified by recrystallization at any temperature or intracrystalline diffusion at temperatures above 200–300 °C (Eiler, 2007; Henkes et al., 2014; Passey & Henkes, 2012; Stolper & Eiler, 2015).

For a hypothetical sample that crystallized at 50 °C then experienced a heating event, it would record a temperature of 50 °C unless the heating event was greater than ~200 °C, in which case it could record the hotter temperature. For temperatures between 100 and 200 °C for calcite (or between 200 and 300 °C for dolomite), partial reordering may occur along the heating path, resulting in recorded temperatures that are lower than peak temperature. A sample that crystallized at 50 °C, then experienced a cooling event, would record a temperature of 50 °C unless the carbonate recrystallized, in which case it would preserve the isotopic signature of the new fluid (Eiler, 2007; Henkes et al., 2014; Passey & Henkes, 2012; Stolper & Eiler, 2015).

3. Methods

Carbonate samples were collected from field sites in Nevada and Wyoming between 2010 and 2013. We took a broad approach to sampling and analyzed a large number of different textures from different locations, with replications focused on a few key samples from the detachment surface. We did this to maximize the probability of finding elevated temperatures from frictional heating, at the expense of more precise temperature values that come from replication. The errors on unreplicated samples presented here are sufficiently small to easily distinguish comminuted host rock material from carbonate that mineralized at temperatures 100–200 °C higher than the host rock.

All samples were analyzed in powder form, with a mass of 8 to 12 mg. Powdered samples of carbonate were primarily obtained by microdrilling (labeled with a T in the sample name, Tables 1 and 2), using a 0.5-mm drill bit, to extract 8–12 mg of carbonate from split or saw cut hand samples. Features smaller than 5 mm are too small to sample separately using this technique. For some samples, multiple drill tracks were obtained, usually targeting different colors or textures within the rock sample. Three samples (labeled with a C in the sample name, Tables 1 and 2) were analyzed as small chips, while 15 others (labeled with an M in the sample name, Tables 1 and 2) were powdered using a mortar and pestle.

Using the sample preparation and analysis techniques described in Huntington et al. (2009), the samples were digested in phosphoric acid at 90 °C to produce CO_2 gas, which was then cleaned by established cryogenic and gas chromatographic methods along an automatic gas handling line, and analyzed using a Thermo MAT 253 gas source mass spectrometer at the California Institute of Technology. Measurements were collected for masses of 44–48 Da per unit charge. The measurements of mass 47, which consists principally of $^{13}C^{18}O^{16}O$, but also minor quantities of $^{12}C^{18}O^{17}O$ and $^{13}C^{17}O_2$, are compared to that expected for a stochastic distribution, and the difference is denoted as Δ_{47}, in units of per mil (Eiler, 2011).

Measured values for Δ_{47} for each sample were normalized to values measured in gases heated to 1,000 °C and then converted into the absolute reference frame either via comparison with concurrently analyzed gases that had been equilibrated with water at 25 °C or via a "secondary transfer function" based on analysis of carbonate standards, as described by Dennis et al. (2011; see also Bergmann, 2013). Then an acid digestion correction of +0.092‰ for a 90 °C acid bath was applied, in order to compare measured Δ_{47} values with temperature calibrations that assume carbonate acid digestion at 25 °C. The corrected Δ_{47} values are empirically related to temperature using experimental data from natural and synthetic calcites, aragonites, and dolomites (Bonifacie et al., 2011, 2013; Passey & Henkes, 2012; Stolper & Eiler, 2015), converted into the absolute reference frame (Max Lloyd, personal communication, 2014; this conversion can be closely approximated by simply translating the high-temperature calibration of Stolper & Eiler, 2015, to the absolute reference frame using the secondary transfer function techniques of Dennis et al., 2011).

Measurements of $\delta^{18}O$ and $\delta^{13}C$ were obtained by comparison to known gases. All stated carbon isotopic ratios are $\delta^{13}C$ with respect to VPDB, and oxygen isotopic ratios are $\delta^{18}O$ with respect to VSMOW. The $\delta^{18}O$ of the pore water in equilibrium with the samples at the time of crystallization ($\delta^{18}O_{water}$) was calculated using fractionation factors from O'Neil et al. (1969) and Vasconcelos et al. (2005). Acid digestion fractionation factors at 90 °C were taken from Guo et al. (2009) and Rosenbaum and Sheppard (1986). For mixed calcite-dolomite samples, all calculations were done for both end-members of pure calcite and pure dolomite, and the $\delta^{18}O_{carbonate}$ and $\delta^{18}O_{water}$ values reflect a weighted average based on estimates of the calcite/dolomite ratios.

Table 1
Isotopic Data for Samples From the Mormon Peak Detachment Area, Sorted by Texture

Sample	Location[a]	$\delta^{13}C$	$\delta^{13}C$ SE	$\delta^{18}O_c$	$\delta^{18}O$ SE	Δ47-ARF	Δ47 SE	T	T + error	T − error	$\delta^{18}O_w$	O_w + error	O_w − error
HW-v													
ES10-21 T4	2	−5.068	0.0019	20.245	0.0030	−0.215	0.030	8	4	3	−12	0.9	0.9
ES10-32 T2	4	−8.022	0.0016	20.038	0.0031	−0.350	0.034	30	5	5	−7	1.0	1.0
ES10-35 T1	4	−7.568	0.0013	18.580	0.0021	−0.324	0.024	20	4	4	−10	1.0	0.9
ES09-04 D1	3	0.776	0.0014	9.217	0.0024	−0.444	0.020	73	9	8	−11	1.1	1.1
ES10-05 D1	1	0.358	0.0005	10.238	0.0027	−0.419	0.012	63	8	7	−11	1.1	1.1
ES10-05 D2	1	0.909	0.0013	12.106	0.0020	−0.409	0.026	68	8	8	−8	1.1	1.1
ES10-22 T2	2	−5.752	0.0010	18.995	0.0022	−0.297	0.024	21	4	4	−10	1.0	0.9
ES10-33 T1	4	−7.798	0.0016	18.333	0.0031	−0.341	0.025	23	5	4	−10	1.0	0.9
FW-v													
ES12-13 T2	6	0.107	0.0009	21.549	0.0012	−0.352	0.030	136	12	11	5	0.9	0.9
ES12-12 T1[c]	6	−0.291	0.0024	21.391	0.0040	−0.532	0.039	144	35	27	6	2.4	2.3
DET-b													
120107-01	5	−1.054	0.0042	18.819	0.0041	−0.500	0.032	114	13	12	0	1.2	1.2
120107-1b	5	0.246	0.0016	23.880	0.0033	−0.316	0.032	104	16	14	4	1.5	1.5
ES12-14	6	1.591	0.0015	13.465	0.0030	−0.373	0.032	77	12	11	−8	1.5	1.4
ES12-14 T4 [c]	6	2.128	0.0041	22.211	0.0055	−0.428	0.039	81	19	16	2	2.2	2.1
ES12-16 T1[c]	6	−0.024	0.0044	21.429	0.0078	−0.521	0.033	135	32	25	5	2.3	2.3
ES10-23 D2	2	−1.057	0.0011	19.124	0.0018	−0.466	0.029	149	18	16	3	1.2	1.2
ES10-23 M5P1	2	−1.804	0.0006	19.306	0.0011	−0.420	0.023	104	12	11	0	1.2	1.2
ES10-23 M5P2	2	−1.796	0.0009	19.268	0.0018	−0.404	0.023	92	11	10	−2	1.2	1.1
ES10-23 M7	2	−1.350	0.0009	20.142	0.0035	−0.259	0.033	29	5	5	−9	1.0	0.9
ES10-25 T5	2	−5.213	0.0012	18.938	0.0011	−0.331	0.035	31	5	5	−8	1.0	1.0
ES10-27 T1	2	−4.085	0.0029	20.303	0.0037	−0.295	0.042	29	5	5	−7	1.0	1.0
ES10-27 T2	2	−4.926	0.0021	18.952	0.0061	−0.286	0.060	20	5	5	−10	1.1	1.1
ES12-13	6, 1 m below det	−0.125	0.0014	21.976	0.0029	−0.366	0.022	125	19	17	5	1.6	1.5
ES12-03 T2	5	−2.871	0.0034	20.894	0.0068	−0.409	0.040	64	8	7	−2	1.1	1.1
ES12-03 T3	5	−2.528	0.0038	21.699	0.0049	−0.471	0.039	97	11	10	3	1.2	1.2
ES12-06 T1	5	−0.344	0.0021	17.523	0.0022	−0.468	0.015	92	11	10	−3	1.2	1.1
ES12-06 T2	5	−0.645	0.0021	15.495	0.0022	−0.547	0.028	140	17	15	−1	1.2	1.2
ES12-06 T3	5	−0.613	0.0042	15.661	0.0056	−0.557	0.046	150	19	16	0	1.3	1.2
ES12-06 T4	5	−0.535	0.0016	15.740	0.0032	−0.470	0.026	148	27	22	0	1.8	1.7
ES12-18	6, 12 m below det	−0.036	0.0015	23.028	0.0023	−0.317	0.030	96	15	13	3	1.5	1.5
ES12-18 T1[c]	6, 12 m below det	−0.089	0.0029	22.810	0.0039	−0.475	0.021	106	24	20	3	2.2	2.2
ES12-18 T2	6, 12 m below det	−0.068	0.0009	22.711	0.0022	−0.356	0.031	134	24	20	6	1.8	1.7
ES12-20	6	−0.120	0.0017	21.765	0.0028	−0.397	0.039	153	25	21	7	1.6	1.6
ES12-19 T4	6	0.447	0.0014	16.942	0.0026	−0.389	0.029	101	17	15	−3	1.7	1.6
ES12-19 T6	6	1.674	0.0018	19.562	0.0037	−0.339	0.037	103	18	15	0	1.7	1.6
ES12-17 T1[c]	6	−0.822	0.0013	21.038	0.0024	−0.458	0.040	88	20	17	0	2.2	2.1
ES12-05 T2	5	−2.568	0.0031	19.908	0.0041	−0.438	0.030	75	9	8	−1	1.1	1.1
ES10-32 T1	4	1.795	0.0018	24.786	0.0020	−0.281	0.034	71	9	8	4	1.2	1.1
DET-g													
ES12-19	6	1.711	0.0012	17.099	0.0027	−0.381	0.027	110	17	15	−2	1.5	1.5
ES12-19 T7	6	1.036	0.0016	12.277	0.0035	−0.432	0.039	92	16	14	−8	1.7	1.6
ES12-01 M1	5	0.898	0.0025	21.222	0.0029	−0.432	0.037	83	10	9	1	1.2	1.1
ES12-10	6	−1.641	0.0014	21.881	0.0040	−0.383	0.044	126	19	17	5	1.6	1.5
ES12-04 T1S2	5	−5.683	0.0039	20.723	0.0053	−0.256	0.025	13	4	4	−10	0.9	0.9
ES12-04 T1S1	5	−5.645	0.0029	20.787	0.0035	−0.202	0.029	3	3	3	−12	0.8	0.8
ES12-04 T2	5	−5.092	0.0038	19.442	0.0055	−0.230	0.037	7	4	3	−13	0.9	0.9
ES12-05 T1	5	−1.622	0.0024	20.266	0.0025	−0.469	0.031	95	11	10	1	1.2	1.2
ES12-11 T1[c]	6	−0.109	0.0026	21.874	0.0040	−0.487	0.046	110	26	21	3	2.3	2.2
ES10-23 M6P1	2	−1.155	0.0029	20.834	0.0114	−0.497	0.018	209	29	24	9	1.3	1.3
ES10-23 M6P2	2	−1.159	0.0019	20.832	0.0053	−0.502	0.029	218	31	26	9	1.3	1.3
ES12-15 T1[c]	6	2.000	0.0019	18.008	0.0043	−0.435	0.022	75	18	15	−5	2.1	2.0
ES10-25 T3	2	−5.345	0.0011	19.160	0.0025	−0.303	0.024	24	5	4	−9	1.0	0.9
ES10-23 T5	2	−1.447	0.0022	20.673	0.0036	−0.453	0.034	126	15	13	3	1.2	1.2
ES10-35 T2[b]	4	−7.052	0.0017	19.169	0.0014	−0.336	0.052	27	5	5	−9	1.0	1.0
ES12-03 T1	5	−4.347	0.0037	19.094	0.0060	−0.367	0.043	43	6	6	−7	1.0	1.0

Notes to Table :

[a]Site number locations shown in Figure 3. Carbon isotopes are with respect to VPDB, oxygen isotopes are with respect to VSMOW, T is temperature in °C; $\delta^{18}O_w$ is the oxygen composition of water in equilibrium with carbonate, with respect to VSMOW; SE is standard error; ARF is in the absolute reference frame. [b]One erroneous acquisition (out of eight) was removed from the calculations. [c]Run during a week of slightly lower than usual analytic precision (difference between calculated and observed Δ47 in carbonate standards was up to.06, rather than the usual <.03).

Proportions of calcite and dolomite varied widely among our samples: host rock, void-fill samples, and veins generally contained pure isolates of one or the other phase (as determined by reaction with dilute hydrochloric acid). Breccias, gouges, and clastic dikes were often mixtures of the two. In these cases, we analyzed a mixture of calcite and dolomite and estimated the contributions of each to that mixture using X-ray diffraction analyses and visual estimates using scanning electron microscopy (SEM) images. However, these measurements were made on portions of the sample that we deemed to be texturally equivalent to the analyzed powders rather than on those powders themselves. Variations across the sample would introduce errors in this estimate. However, even errors as large as 20% would change the calculation of $\delta^{18}O$ of carbonate by no more than 0.5‰ and the $\delta^{18}O$ of water by 1‰. Temperatures calculated from clumped-isotope measurements are not noticeably affected by the calcite/dolomite ratio (Stolper & Eiler, 2015).

Errors are 1-sigma standard errors of the mean, based on the cumulative results of eight acquisitions of 7 cycles per acquisition. These errors range from 0.0004‰ to 0.011‰ (averaging 0.003‰) in the carbon and oxygen isotope measurements and from 0.004‰ to 0.021‰ (averaging 0.012‰), for Δ_{47}. These errors in Δ_{47} are generally consistent with the expectations of shot-noise errors (i.e., they are limited by mass spectrometric counting statistics) and propagate into errors in temperature of ±2 to 112 °C, depending on the temperature, with the majority of samples under 100 °C having errors of 2 to 10 °C and the majority of samples between 100 and 200 °C having errors of 12–30 °C. Temperatures of greater than 200 °C have larger errors (50–112 °C) but are sufficient to distinguish between the groups discussed here.

The temperatures presented here are calculated under the assumption of equilibrium conditions during precipitation or recrystallization. This is likely not entirely correct, both due to the possibility of kinetic isotope effects during mineral growth and due to partial resetting of the thermometer during heating to temperatures between 100 and 200 °C for calcite and 200–300 °C for dolomite, which would lead these recorded temperatures to be underestimates of the actual temperatures. Despite these ambiguities, systematic trends in our results suggest that these "apparent" temperatures offer some insight into formation conditions for different textures within a fault zone and in particular preserve evidence for frictional heating along faults.

We first describe the sampling strategy and types of sample textures common to both sites (the Mormon Peak detachment and the Heart Mountain detachment). We then present the geologic setting, isotopic results, and discussion for each site. We then compare the two sites and present our conclusions.

4. Sample Texture Descriptions

Samples collected from the damage zones of the Mormon Peak and Heart Mountain detachments display a variety of textural features. We summarize these features below and show typical examples in Figures 1 and 2. For more comprehensive structural characterization of these damage zones, including extensive documentation of features directly related to fluid flow such as veins and stylolites, we refer the reader to Anders et al. (2006), Anderson et al. (2010), Diehl et al. (2010), and Swanson et al. (2012) for the Mormon Peak detachment and Anders et al. (2010) and Swanson et al. (2016) for the Heart Mountain detachment.

We stress here that the damage zones along both these detachments do not exhibit rock fabric (i.e., systematically oriented geologic features) at either outcrop or regional scale. Although such fabrics may arise on brittle structures (e.g., Snoke et al., 1998), for the Mormon Peak and Heart Mountain damage zones, the randomizing effect of cataclasis (e.g., Sibson, 1977; effectively, an ongoing "structural explosion") largely has destroyed any coherent fabrics that may have temporarily developed. One might attempt, in theory,

Table 2
Isotopic Data for Samples From the Heart Mountain Detachment Area, Sorted by Texture

Sample	Location[a]	$\delta^{13}C$	$\delta^{13}C$ SE	$\delta^{18}O_c$	$\delta^{18}O$ SE	Δ47-ARF	Δ47 SE	T	T + error	T − error	$\delta^{18}O_w$	O_w + error	O_w − error
host													
ES-HM12-18 T1	SG	3.679	0.0026	26.705	0.0045	0.606	0.012	51	11	10	3	1.7	1.6
BW-HM12-10	host	−1.247	0.0007	22.635	0.0014	0.616	0.015	48	7	7	−4	1.1	1.1
ES-HM12-34 T1	HM	−1.776	0.0016	23.637	0.0030	0.595	0.010	55	8	7	−1	1.2	1.1
ES-HM13-02 T1	SF	2.847	0.0011	22.160	0.0024	0.643	0.012	39	7	7	−3	1.3	1.3
ES-HM12-24 T2	CC	−0.442	0.0014	22.437	0.0016	0.583	0.011	60	5	5	−3	0.8	0.8
ES-HM12-24 T4	CC	−0.441	0.0008	22.753	0.0011	0.612	0.014	49	5	5	−4	0.8	0.8
FW-v													
ES-HM12-27 M1	CC	−0.039	0.0007	22.398	0.0014	0.597	0.011	55	5	5	−3	0.8	0.8
DET-b													
ES-HM13-37 T2	FC	−1.007	0.0014	22.279	0.0021	0.601	0.013	53	5	5	−4	0.8	0.8
ES-HM13-38	FC	−0.922	0.0018	20.075	0.0014	0.728	0.019	17	4	4	−10	1.0	0.9
ES-HM13-37 T1	FC	−0.982	0.0018	22.311	0.0021	0.613	0.018	49	7	6	−4	1.0	1.0
ES-HM13-37 T3	FC	−1.184	0.0014	22.404	0.0028	0.586	0.009	59	6	5	−3	0.8	0.8
ES-HM13-06 T1	SHP	−0.625	0.0012	23.910	0.0034	0.597	0.006	55	9	8	−2	1.3	1.3
ES-HM13-28 T1	CR	1.324	0.0008	21.047	0.0022	0.557	0.016	71	11	10	1	1.4	1.4
ES-HM12-20 T3	CC	−0.431	0.0030	22.518	0.0060	0.601	0.007	53	5	5	−4	0.8	0.8
ES-HM12-20 T1	CC	0.629	0.0007	20.266	0.0019	0.562	0.008	69	6	6	−4	0.8	0.8
ES-HM12-14 T2	SG	3.949	0.0012	29.974	0.0022	0.601	0.010	53	8	7	7	1.2	1.2
ES-HM12-31 T3	SB	−1.317	0.0012	24.925	0.0025	0.567	0.012	67	6	6	1	0.8	0.8
ES-HM12-31 T1	SB hw	−1.355	0.0011	25.643	0.0010	0.556	0.009	72	6	6	2	0.8	0.8
ES-HM12-15	SG	−1.425	0.0012	24.386	0.0022	0.579	0.017	62	8	8	−1	1.2	1.2
ES-HM12-09 T2	JS	−1.574	0.0013	17.614	0.0029	0.562	0.015	69	9	8	−4	1.2	1.2
ES-HM12-10 M1	JS fw	−3.086	0.0007	11.964	0.0020	0.604	0.013	52	5	5	−12	0.8	0.8
ES-HM12-21 T4	CC	−1.417	0.0014	22.021	0.0012	0.563	0.010	69	6	6	−2	0.8	0.8
ES-HM12-07 T2	JS fw	−1.539	0.0018	15.864	0.0027	0.553	0.010	73	6	6	−6	0.8	0.8
ES-HM12-12 T1	JS	−1.999	0.0018	22.573	0.0040	0.572	0.015	65	13	11	−2	1.7	1.6
ES-HM12-09 T1	JS	−1.266	0.0017	22.533	0.0032	0.568	0.017	66	9	8	0	1.2	1.2
ES-HM12-09 T5	JS fw	−1.281	0.0011	24.060	0.0013	0.584	0.006	60	5	5	0	0.8	0.8
ES-HM12-09 T3[b]	JS	−1.998	0.0019	22.366	0.0032	0.632	0.013	43	7	6	−4	1.1	1.1
ES-HM12-09 T4	JS fw	−1.833	0.0012	23.995	0.0011	0.586	0.013	59	6	5	0	0.8	0.8
ES-HM12-21 T1	CC	1.389	0.0008	22.821	0.0020	0.550	0.013	75	6	6	0	0.8	0.8
DET-m													
ES-HM12-06 T2	WM	−2.180	0.0017	22.627	0.0030	0.396	0.013	198	44	34	13	2.1	2.0
ES-HM12-06	WM	−2.113	0.0014	22.681	0.0027	0.347	0.008	284	53	41	17	1.5	1.5
ES-HM12-04 T2	WM	−2.353	0.0016	22.613	0.0029	0.386	0.013	211	44	34	14	1.9	1.9
ES-HM12-06 T5	WM	−2.659	0.0014	21.472	0.0026	0.374	0.013	231	51	38	14	2.0	1.9
TH-HM12-01	WM	−2.765	0.0018	26.463	0.0020	0.463	0.010	128	17	15	12	1.4	1.3
ES-HM12-03 T1	WM	−2.221	0.0015	22.447	0.0022	0.355	0.009	267	73	51	16	2.2	2.1
HW-c													
ES-HM13-01 T2	SF	−1.928	0.0008	18.521	0.0032	0.640	0.012	40	7	7	−7	1.3	1.3
ES-HM12-13 T1	JS	−1.289	0.0010	12.112	0.0008	0.602	0.010	53	5	5	−12	0.8	0.8
ES-HM13-41 TD	FC	−0.482	0.0011	24.585	0.0025	0.643	0.014	39	4	4	−4	0.8	0.8
ES-HM13-41 TE	FC	−0.553	0.0004	24.779	0.0018	0.625	0.012	45	5	5	−2	0.8	0.8
ES-HM13-41 TF	FC	−0.555	0.0011	24.922	0.0021	0.627	0.010	44	5	5	−2	0.8	0.8
ES-HM13-41 TA2	FC	−0.479	0.0011	24.983	0.0025	0.587	0.006	59	6	5	0	0.8	0.8
ES-HM13-41 TB2	FC	−0.466	0.0007	24.961	0.0021	0.598	0.009	54	5	5	−1	0.8	0.8
ES-HM13-41 TC2	FC	−0.525	0.0007	25.006	0.0014	0.594	0.006	56	6	5	0	0.8	0.8
ES-HM13-39	FC	−0.699	0.0018	22.327	0.0028	0.619	0.011	47	5	5	−3	0.8	0.8
ES-HM13-29 T1	CR	−0.254	0.0019	24.496	0.0045	0.558	0.010	71	11	10	4	1.4	1.4
ES-HM13-24 T2	CR	−1.037	0.0018	21.027	0.0029	0.529	0.007	85	13	11	1	1.5	1.4
ES-HM12-23 T1	CC	−0.940	0.0012	10.490	0.0013	0.557	0.009	72	6	6	−12	0.8	0.8
ES-HM12-23 T3	CC	0.367	0.0008	22.207	0.0012	0.573	0.011	64	6	5	−2	0.8	0.8
ES-HM12-19a M1	SG	0.513	0.0016	12.879	0.0035	0.589	0.014	58	9	8	−11	1.3	1.3
HW-v													
ES-HM12-05	WM	2.584	0.0017	22.136	0.0031	0.717	0.008	19	5	4	−7	1.0	1.0
ES-HM12-41 C2	HM	−3.276	0.0015	15.408	0.0031	0.618	0.009	47	7	6	−8	1.1	1.1
ES-HM12-41 C1	HM	−3.433	0.0017	15.444	0.0029	0.606	0.006	51	7	7	−8	1.2	1.1
ES-HM13-35 T1	FC	−2.122	0.0022	15.605	0.0068	0.612	0.010	49	8	8	−8	1.3	1.3
ES-HM13-30 T1	CR	−1.262	0.0015	11.862	0.0028	0.630	0.010	43	8	7	−13	1.3	1.3

Table 2 *(continued)*

Sample	Location[a]	$\delta^{13}C$	$\delta^{13}C$ SE	$\delta^{18}O_c$	$\delta^{18}O$ SE	Δ47-ARF	Δ47 SE	T	T + error	T − error	$\delta^{18}O_w$	O_w + error	O_w − error
ES-HM13-08 C1	SHP	−1.368	0.0017	11.798	0.0035	0.571	0.015	65	10	9	−9	1.4	1.4
HW-f													
ES-HM12-41 T2	HM	−2.090	0.0012	19.555	0.0025	0.493	0.016	106	14	12	2	1.3	1.3
ES-HM12-39 M1	HM	−2.713	0.0017	20.180	0.0042	0.454	0.016	135	20	17	4	1.5	1.5
ES-HM12-35 T3	HM	−1.777	0.0012	20.418	0.0038	0.512	0.009	94	14	12	1	1.5	1.5
ES-HM12-34 T4	HM	−2.733	0.0013	17.405	0.0054	0.474	0.010	119	18	16	1	1.5	1.5
ES-HM12-35 T4	HM	−2.667	0.0013	20.648	0.0037	0.458	0.017	132	20	17	5	1.6	1.5
ES-HM12-34 T3	HM	−2.136	0.0014	21.098	0.0039	0.547	0.013	76	12	10	0	1.4	1.4
ES-HM12-33a M1	SB	−0.619	0.0021	26.219	0.0060	0.533	0.013	83	12	11	4	1.4	1.4
ES-HM12-34 T2	HM	−1.212	0.0022	23.500	0.0032	0.379	0.017	222	35	29	14	1.5	1.4
ES-HM12-32 T1	SB	−0.148	0.0016	25.287	0.0030	0.521	0.011	89	17	14	4	1.8	1.7
ES-HM12-41 T1	HM	−0.865	0.0018	23.816	0.0046	0.514	0.017	93	12	11	5	1.3	1.3
ES-HM12-35 T1	HM	−2.634	0.0011	19.878	0.0043	0.474	0.011	119	18	16	3	1.5	1.5
ES-HM12-35 T2	HM	−1.835	0.0009	21.667	0.0022	0.282	0.012	573	318	147	19	1.9	1.8
ES-HM12-35 T5	HM	−2.557	0.0015	21.103	0.0035	0.353	0.012	270	58	43	13	1.7	1.7
ES-HM12-35 T6	HM	−1.379	0.0014	21.439	0.0020	0.339	0.010	303	84	57	13	2.0	1.9
HW-g													
ES-HM12-16 M3	SG	2.421	0.0015	28.304	0.0025	0.600	0.016	54	8	7	5	1.2	1.2
ES-HM12-32 T2	SB	−0.754	0.0017	26.785	0.0044	0.422	0.011	166	34	27	12	2.0	1.9
ES-HM12-39 M2	HM	−2.829	0.0028	19.892	0.0046	0.405	0.010	186	31	25	7	1.6	1.6
ES-HM12-33a T1	SB	−0.571	0.0020	23.916	0.0031	0.527	0.012	86	16	14	2	1.8	1.7
ES-HM12-40	HM	−2.415	0.0012	19.498	0.0025	0.426	0.011	161	33	26	5	2.0	1.9
ES-HM12-30 M1	SB	−0.599	0.0023	24.147	0.0043	0.618	0.011	47	8	7	−3	1.3	1.3
ES-HM13-43 T1	DH	3.222	0.0020	29.039	0.0042	0.643	0.013	39	7	7	3	1.3	1.3
ES-HM13-42 T1 S1	DH	−0.041	0.0018	26.425	0.0046	0.545	0.013	77	12	10	7	1.5	1.4
ES-HM13-19H T2	HM	2.268	0.0011	30.409	0.0028	0.622	0.013	46	8	7	3	1.3	1.3
ES-HM12-40 M1	HM	−1.518	0.0015	17.789	0.0035	0.697	0.011	24	5	5	−12	1.0	1.0
ES-HM13-44 T1	DH	2.675	0.0034	30.782	0.0034	0.636	0.017	41	8	7	6	1.3	1.3
ES-HM13-12 T1	SHP	−1.502	0.0021	25.371	0.0039	0.558	0.018	71	11	10	2	1.4	1.4
ES-HM13-19H T1	HM	3.181	0.0021	30.415	0.0038	0.611	0.014	50	8	8	4	1.3	1.3

[a]Site locations shown in Figure 5, except host which is from Rattlesnake Anticline; HW refers to hanging wall; FW refers to footwall. Carbon isotopes are with respect to VPDB, oxygen isotopes are with respect to VSMOW, T is temperature in °C; $\delta^{18}O_w$ is the oxygen composition of water in equilibrium with carbonate, with respect to VSMOW; SE is standard error; ARF is in the absolute reference frame. [b]One erroneous acquisition (out of eight) was removed from the calculations.

to relate individual isotopic measurements (e.g., on various generations of vein fill) to a regional history of deformation, based on superposition of variably oriented fabric elements, analogous to zones of metamorphic tectonites. For the present study, no such analysis was attempted.

The Mormon Mountains sampling was focused exclusively on the detachment zone, and all fault-related samples were collected from within a meter of the main slip surface (except two samples, ES12-13 and ES12-18, as noted in Table 1). Sampling within the Heart Mountain area targeted both the detachment zone and tectonically associated hanging wall structures 5 to 40 m above the main fault. We distinguish the samples here using abbreviations keyed to their locations relative to the detachment surface, with "FW" referring to the footwall, "DET" referring to the detachment plane and samples within c. 10 cm of it, and "HW" referring to the hanging wall, and "host" referring to samples unaffected by faulting.

Host rock samples (host): These samples were collected from areas away from fault deformation, to establish a baseline for fault-related effects. In the Mormon Mountains, host rock data were previously reported in Swanson et al. (2012) but are discussed again here in comparison to Heart Mountain area samples. Host rocks from the Mormon Peak detachment area were collected from Cambrian strata 250 to 300 m structurally below the detachment. In the Heart Mountain detachment area, host rocks were collected from a few different areas. Ordovician Bighorn Formation samples were collected from the Rattlesnake anticline, at least 1 km below any potential eroded detachment surface, and 5 km east of the southeasternmost exposures of the detachment. In addition, samples were collected from (1) the Mississippian Madison Formation 10 m above the detachment, near the northwesternmost exposure of the detachment, and (2) from the footwall near the center of detachment exposures in the Cambrian Grove Creek Formation, at least 15 m

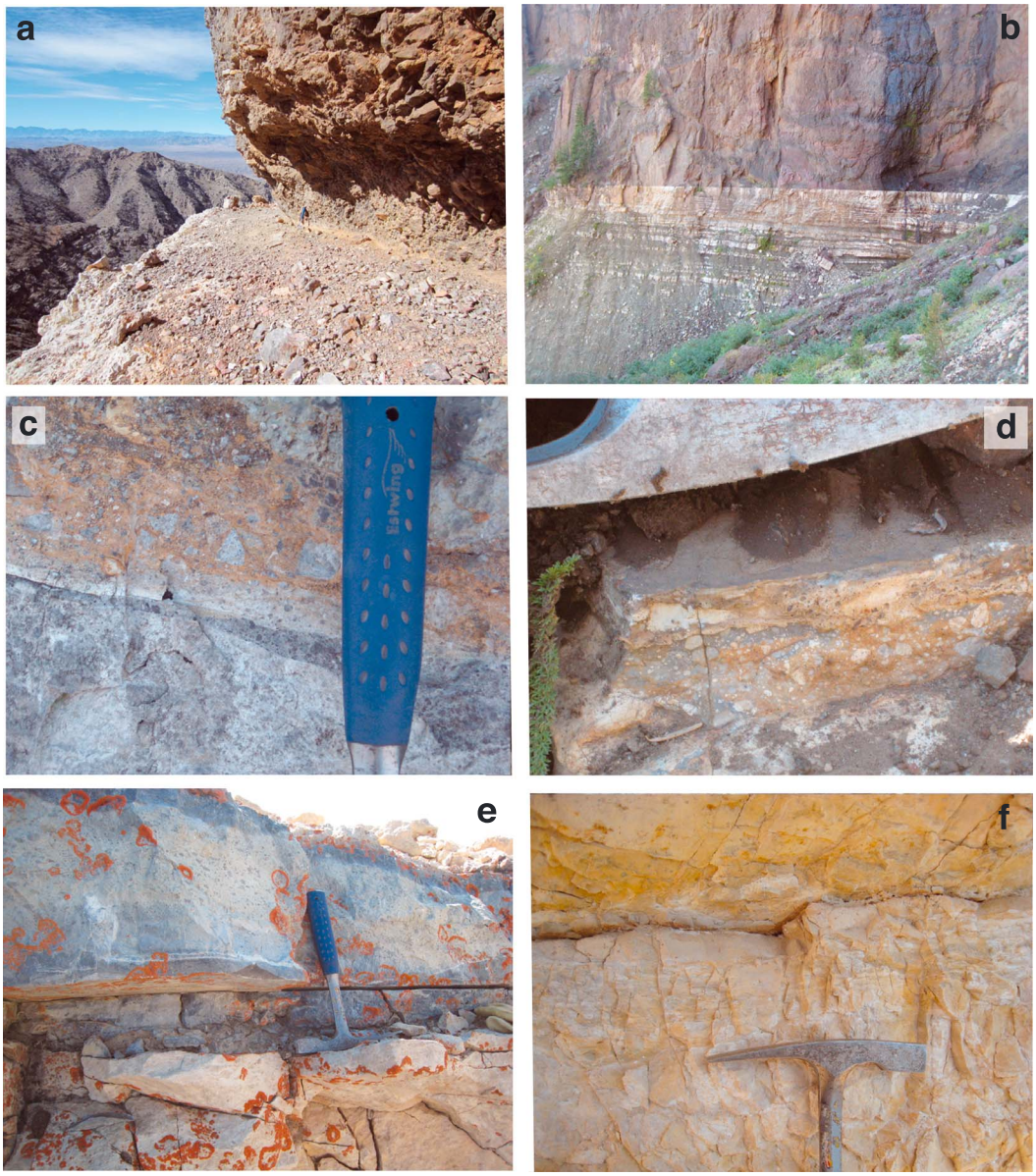

Figure 1. Photographs showing the context and representative textures of fault rocks along the (a, c) Mormon Peak and (b, d, e, and f) Heart Mountain detachments. (a) An exposure of the Mormon Peak detachment, showing preferential erosion of the brecciated hanging wall. Thin light brown detachment plane is about 2 m below the top of the shadow. (b) An exposure of the Heart Mountain detachment at Jim Smith Creek, with a ~35-m thickness of dark brown hanging wall volcanics in the top half of the frame. (c) Photo of the breccia along the Mormon Peak detachment (DET-b), with the main slip surface at the top of the dark gray wedge. Hammer handle is c. 15-cm long. (d) Photo of breccia along the Heart Mountain detachment at Jim Smith Creek (DET-b), dark, shadowed surface is a veneer of the hanging wall over the top of the breccia. Width of view is 6 cm. (e) Photo of a hanging wall fault breccia at Heart Mountain (HW-f). Hammer is 28-cm long. (f) Photo of hanging wall fault breccia at Steamboat, Heart Mountain detachment. Head of hammer is 18-cm long.

below the detachment. These samples did not show evidence, at outcrop scale, of being deformed by the detachment.

Footwall veins (FW-v): These are samples of calcite spar that precipitated in cracks that formed within a meter of the detachment. Only veins of at least 2-mm width could supply enough material to analyze, limiting the number of these analyses.

Detachment breccia (DET-b): These samples were all collected from within 1 m of the detachment surfaces (except ES12-18, at 12 m below the detachment) and predominantly within 10 cm. They consist of a

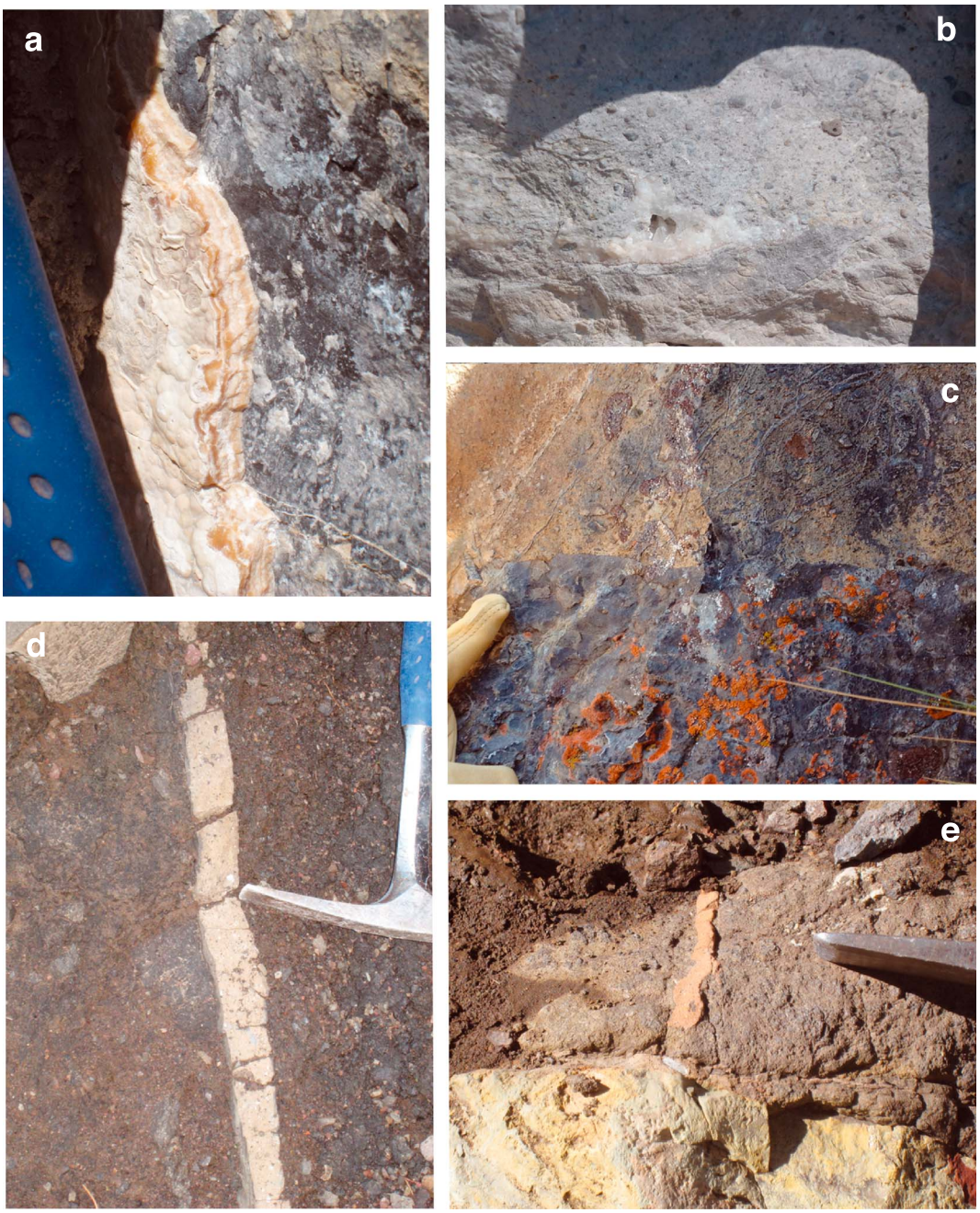

Figure 2. Photographs of examples of sample types: (a) hanging wall vein (HW-v), about 1 cm in width from White Mountain, and (b) hanging wall void fill (HW-v) from Heart Mountain, with calcite spar filling an irregular void in a breccia. Width of view is approximately 10 cm. (c) The basal layer breccia at White Mountain, where the hanging wall is metamorphosed to marble (DET-m). Height of view is 26 cm. (d) Clastic dike (HW-c) from Jim Smith Creek, with maximum width of 3 cm. (e) Smaller clastic dike (HW-c), c. 8 mm in width, just above the detachment (base of dark gray volcanic hanging wall) at Jim Smith Creek, but not continuous with it within the plane of the photo.

fine-grained matrix and angular clasts (Figures 1a, 1c, and 1d), some of which appear to be clasts of an earlier brecciation episode Figure 6 in Swanson et al., 2016). An attempt was made to avoid large clasts when sampling, to aim for a more homogenous mixture of matrix material. The breccia varied widely from many meters thick and highly visible from up to 100 m away (e.g., Figure 1a) to under 1-cm thick and barely detectable from 100 m away (Figure 1b; see also Swanson et al., 2016).

Marble breccia (DET-m): These samples are exclusively from the unique basal cataclasite at White Mountain (Heart Mountain allochthon), where all of the hanging wall host is metamorphosed by local intrusions. These breccias were sampled from within 3 m of the detachment, but their distinctive appearance and proximity to metamorphic and magmatic features lead us to consider them separately from other detachment breccias (Figure 2c).

Gouge (DET-g for Mormon Mountains and HW-g for Heart Mountain allochthon): These samples are very fine-grained cataclasites with no clasts visible, even with an optical microscope. The Mormon Mountains gouge samples were collected from the detachment surface, while the Heart Mountain gouge samples were collected from hanging wall faults, due to lack of carbonate-rich gouges along the detachment surface.

Hanging wall veins, void fills, and calcrete (HW-v): These hanging wall veins and void fills are sparry calcite (Figures 2a and 2b) and dolomite (dolomite-filled fractures are interpreted to be unrelated to the deformation events of interest here but are included for comparison). Veins fill parallel-sided, but often nonplanar, fractures that are between 2 mm and 2 cm wide, while void fills have irregular boundaries and may be up to decimeter scale. Two of the veins at Heart Mountain show growth fibers in the calcite that are perpendicular to the vein edge, although their lack of deformation suggests that these may have formed postdetachment. This category also includes vein material that is fine grained and texturally similar to calcrete. These samples were collected and analyzed to gain insight into the source of fluids present near the detachment.

Clastic dikes (HW-c): These samples are texturally and lithologically similar to detachment breccias but are found in irregular dike-like structures at high angles to the detachment. They are thought to be formed by processes similar to detachment breccias, before being injected into neighboring rock. These were only collected from the Heart Mountain allochthon, where their identification was greatly facilitated by the contrast in color with the dark volcanic host rock (see Figures 2d and 2e).

Hanging wall fault breccia (HW-f): These cataclastic rocks were sampled from faults contained entirely within the hanging wall. These were only sampled from the Heart Mountain allochthon. Samples contain both matrix material and small clasts of original carbonate and older breccias (Figure 1e). Large clasts, if present, were avoided during sampling.

5. Mormon Peak Detachment (MPD)

5.1. MPD Geologic Background

The Mormon Peak detachment in Nevada, USA, is an extensively exposed low-angle slip surface, active during middle Miocene extension in the Basin and Range province (Axen et al., 1990; Bidgoli et al., 2015; Swanson & Wernicke, 2017; Wernicke et al., 1985; Figure 3a). The detachment cuts a preexisting thrust fault, part of the frontal décollement zone of the Mesozoic-age Sevier fold-and-thrust belt (Figures 3b and 3c). The footwall of the detachment is unmetamorphosed and relatively intact structurally and includes a thrust plate of Cambrian strata structurally overlying subthrust Cambrian through Mississippian strata resting nonconformably on early Proterozoic basement. Cambrian through Middle Devonian strata are predominantly dolostone, whereas Upper Devonian and younger strata are primarily limestone, each with variable but relatively minor amounts of chert and siliciclastic strata.

The hanging wall of the detachment (Figure 3c) contains Cambrian through Permian carbonates derived from the thrust sheet, locally overlain by late Oligocene to middle Miocene (c. 23–14 Ma) volcanic and sedimentary strata, all displaced westward >10 km relative to footwall rocks (Anderson et al., 2010; Swanson & Wernicke, 2017; Wernicke et al., 1985). Where present, Tertiary strata are approximately concordant with the underlying Paleozoic rocks and include interstratified scarp breccias and Miocene ash flow tuffs. The structural depth of the base of hanging wall blocks prior to faulting and tilting was, therefore, not significantly greater than the total stratigraphic thickness of Tertiary and Paleozoic units, which is about 2,000 m (Figure 3b). Thus, fault-related textures within hanging wall samples were less than 2 km deep at the time of their formation. Exposures of the detachment span an east-west distance of more than 20 km, corresponding to footwall paleodepths of 2 to 7 km, progressively increasing from east to west. We collected samples from six locations that are relatively evenly spaced across this transect (Figure 3a), generally within 1 m of the detachment surface.

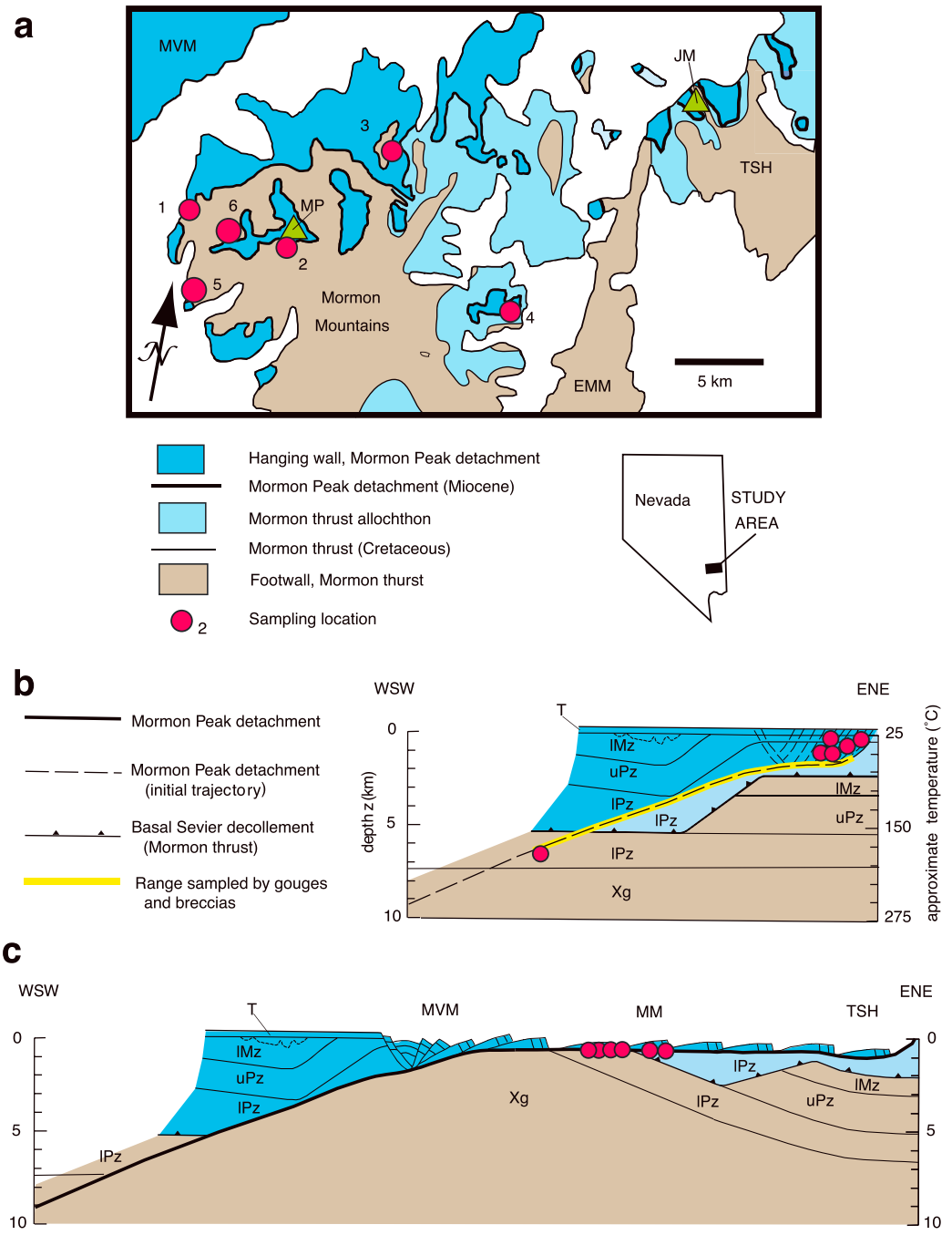

Figure 3. Structural map and schematic cross section of the Mormon Mountains, Nevada, modified from Axen et al. (1990) and Swanson and Wernicke (2017). (a) Map showing the sample locations. MVM, Meadow Valley Mountains; MP, Mormon Peak; JM, Jumbled Mountain; TSH, Tule Spring Hills; EMM, East Mormon Mountains. (b) Reconstructed cross section. Xg, pre-Cambrian basement; lPz, Cambrian-Mississippian strata; uPz, Pennsylvanian and Permian strata; lMz, Triassic through Jurassic strata; T, Tertiary volcanic strata. (c) Simplified postdetachment geometry.

5.2. MPD Isotopic Data

A summary of the 54 new isotopic analyses made in this study for samples from the Mormon Mountains can be found in Table 1 and are plotted in Figure 4, keyed by texture. In addition, we include 42 additional analyses from Swanson et al. (2012), assigned to the new textural categories defined here (shown as smaller symbols with gray outlines in Figure 4). They are discussed below, from footwall to hanging wall.

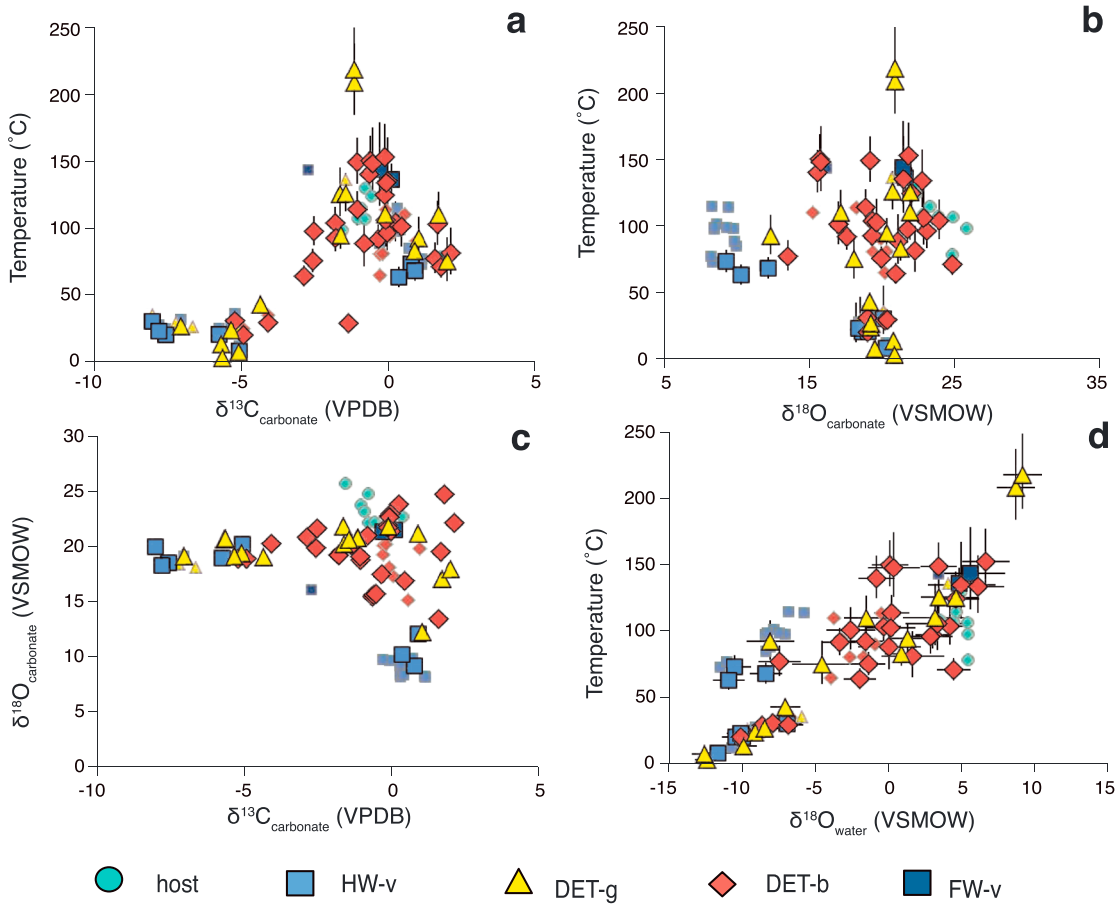

Figure 4. Isotopic data for samples from the Mormon Mountains, Nevada, keyed by texture. Errors are 1-sigma standard errors and smaller than the symbol size for $\delta^{18}O_{carbonate}$ and $\delta^{13}C$ analyses. Smaller symbols without black outlines indicate data previously published in Swanson et al., 2012. HW, hanging wall; FW, footwall; DET, detachment; g, gouge; b, breccia; v, vein material.

Host rock samples (host) have $\delta^{18}O$ values of 22 to 26‰, $\delta^{13}C$ values of −2 to 2‰, clumped-isotope apparent temperatures of 80 to 130 °C, and calculated fluid $\delta^{18}O$ values of 3 to 6‰. These values are consistent with the result of burial diagenesis and/or dolomitization within the Paleozoic or Mesozoic cratonic platform margin.

Footwall veins (FW-v) have $\delta^{18}O$ values of 16 to 22‰, $\delta^{13}C$ values of −3 to 0‰, apparent temperatures of 136 to 144 °C, and calculated fluid $\delta^{18}O$ values of 3 to 6‰. These temperatures are warmer than the surrounding host rock and suggest formation at depths of ~5 km, assuming a Miocene geothermal gradient of approximately 25 °C/km (Bidgoli et al., 2015).

Detachment breccias (DET-b) have $\delta^{18}O$ values of 13 to 25‰, $\delta^{13}C$ values of −6 to 3‰, apparent temperatures of 20 to 153 °C, and calculated fluid $\delta^{18}O$ values of −10 to 7‰. To first order, these remarkably large ranges appear to reflect variations in the proportions of breccia source materials (e.g., host rock, veins and void fills) that differ in isotopic composition.

Gouge samples (DET-g) have $\delta^{18}O$ values of 12 to 22‰, $\delta^{13}C$ values of −8 to 2‰, equilibrium temperatures of 3 to 218 °C, and calculated fluid $\delta^{18}O$ values of−13 to 9‰. These large ranges are similar to those of the breccias and probably also reflect the variable proportions of diverse materials (e.g., host rock, veins, and void fills) contained within these mixtures (see Table 3; also discussed below). One notable difference between the gouge samples (DET-g) and the breccia samples (DET-b) is that the maximum temperature recorded in the gouge samples is 60–75 °C warmer than the maximum temperatures recorded in the breccia samples (210–215 °C versus 140–150 °C).

Table 3
Summary of the three types of materials found in fault breccias and gouges associated with the Heart Mountain (HMD) and the Mormon Peak (MPD) detachments

Material type	Host rock	Syntectonic or immediately posttectonic	Authigenic fault carbonate from fluids
Grain size	10–100 μm	Submicron to 10 μm (?)	Submicron to millimeter
Mineralogy	Dolomite, local calcite in M/D units	both	Generally calcite, local dolomite
Temperature	40–60° for HMD 80–125° for MPD	Closure temperatures, 200 °C+	Ambient: 100 °C or less, depending on depth
$\delta^{18}O$ water	~0‰	Closed system, so dependent on T	Between −12‰ and ~0‰
$\delta^{13}C$	−2 to +2‰ generally, 4‰ for Madison	Same as host	Same as host or may be depleted
Ideal preservation conditions	Away from fault	Older splay of main fault, hanging wall faults	Veins and void fills

Note. M/D refers to Mississippian and Devonian; Madison refers to rocks of the Mississippian Madison Group.

Hanging wall veins, void fills, and calcrete (HW-v) contain carbonate with $\delta^{18}O$ values of 8 to 21‰, $\delta^{13}C$ values of −8 to 1‰, apparent temperatures of 8 to 115 °C, and calculated fluid $\delta^{18}O$ values of −12 to −5‰. These highly depleted values of $\delta^{18}O_{water}$ are indicative of a meteoric water source for these materials. The temperature variations potentially reflect differences in depth at the time of formation, with deeper samples being warmer and shallower samples being colder. The lowest-temperature samples (<20 °C) line modern fractures and show no tectonic offsets or comminution, indicating precipitation after the latest fault-related deformation. We found no additional void fill samples with moderately elevated temperatures, thought to result from up-fault migration of fluids, as presented in Swanson et al. (2012).

5.3. MPD Discussion

In order to determine if samples have been altered by heating, a solid understanding of the source materials is necessary. The gouge and breccia samples are mixtures of carbonates in contact with the fault. This would likely be primarily host rock but could include other material, including veins. Here we consider a variety of trends in the isotopic data from the Mormon Peak detachment that shed light on both the source materials and their heating history (Figure 4).

The coldest samples (<60 °C) also tend to be the most depleted in ^{13}C, with $\delta^{13}C$ values of −5 to −10‰. In addition, they would have been in equilibrium with low $\delta^{18}O_{water}$ (−12 to −6‰) during formation. This supports the interpretation that these carbonates (which are all predominantly calcite) precipitated at relatively shallow depths, where water may include biogenic carbon that is depleted in ^{13}C.

There are two distinct sets of vein and void fill compositions (HW-v) apparent in Figure 4d. One set falls within the cold, ^{13}C-depleted group described above, and the other is a moderate-temperature (70–110 °C) set, depleted in ^{18}O relative to all the other sample types. Both of these sets of veins and void fill samples are calculated to be in equilibrium with low-$\delta^{18}O$ water, presumably meteoric, at crystallization. This is consistent with crystallization within hanging wall veins at different depths (and therefore different temperatures) during the progression of slip. However, the bimodal nature of these samples, rather than the continuous spectrum expected for samples of varying depths, is difficult to explain. Perhaps it is a result of sample preservation or collection bias, as the higher-temperature set came exclusively from one area (sample Site 3 in Figure 3a). Additional sampling may show a continuous variation in temperature.

The gouge and breccia samples (DET-b and DET-g) have compositions either similar to the host rock or between the host rock and vein fill values (apparent in Figure 4c, the plot of $\delta^{13}C$ versus $\delta^{18}O_{carbonate}$). These samples thus show carbon and oxygen isotopic compositions that could result from variable mixtures of the host rock, warm vein material, and cold vein material. But clumped-isotope thermometry data indicate that this is not the case. In the cross plots containing temperatures (Figure 4), some of those mixtures have temperatures that fall outside the range of host rock or either vein set (mixing processes can generate Δ_{47} changes but are contraindicated here because the high-temperature samples do not lie on a mixing line between the lower temperature end-members, discussed in Defliese and Lohmann, 2015). This indicates a source of high-temperature material, discussed in detail below.

The highest-temperature carbonate samples, 209–218 °C, have calculated $\delta^{18}O_{water}$ that is enriched relative to all other samples, with values of up to 9‰ (and up to 19‰ for Heart Mountain samples; see below). It is likely these fluids were heavily rock buffered, such as occurs with a very low water-to-rock ratio in a closed

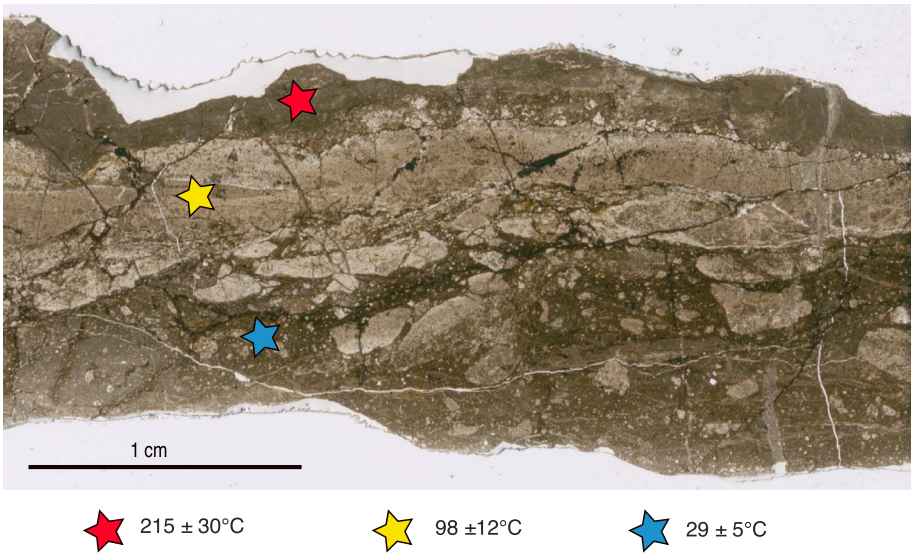

Figure 5. Thin section scan of sample ES10-23, showing three layers of foliated cataclasite along the Mormon Peak detachment plane, each with a distinct texture and temperature.

system. Alternatively, they may reflect the reordering of dolomite at temperatures above 200 °C without the effect of fluids. Either way, it is not likely that these calculated values characterize any large volumes of water.

The samples with the highest temperatures measured in the Mormon Mountains have similar $\delta^{13}C$, $\delta^{18}O$ compositions, and similar calcite/dolomite ratios as host dolomite samples (Figure 4c). The only distinguishing feature is the higher temperature. This highlights the importance of carbonate clumped-isotope thermometry for distinguishing this material from mixtures of host rock and vein material.

The highest temperatures (209–218 °C) are recorded from a sample of a thin (c. 1 cm) layer of gouge collected from the main slip surface near Mormon Peak (ES10-23, Figure 5). This sample shows three layers parallel to the detachment slip surface that are distinct in texture and color in hand sample and in thin section. Each layer has similar oxygen and carbon isotopic compositions ($\delta^{18}O$ values of 19.1–20.1‰ and $\delta^{13}C$ values of −1.1 to −1.8‰), but strongly contrasting temperatures, with the bottom layer averaging 30 °C, the middle layer averaging 100 °C, and the top layer averaging 215 °C. X-ray diffraction analyses indicate that this top layer is nearly pure dolomite, with no trace of Ca or Mg oxides or hydrated oxides that might be expected from decarbonation reactions. SEM imagery shows an extremely fine grain size, with individual grains not well resolved even at micron scale. The middle layer is compositionally and isotopically identical to the host rock, but calcite microveins crosscut the layer, which also contains local euhedral iron oxides. The lower, colder layer shows a larger variety of textures and materials, with the predominant carbonate mineral being calcite. Calcite is present in crosscutting veins, as well as in the breccia matrix. The cold layer contains a clast of the middle layer within it and is therefore younger, but there are no clear crosscutting relationships between the middle layer and the warmest layer.

The recorded c. 200 °C temperature difference thus occurs over a length scale of less than 1 cm, in a sample directly on the detachment surface. The 215 ± 30 °C temperature is hotter than ambient conditions the fault rock would have experienced, with the footwall at that location predicted to have been no deeper than ~4–5 km (Axen et al., 1990; Swanson & Wernicke, 2017). With a surface temperature of 25 °C and a geothermal gradient of 25 °C/km, ambient temperatures would be expected to be 150 °C or colder (e.g., Figure 10a in Bidgoli et al., 2015). Our preferred explanation for the formation of this hot layer is grain size reduction over several slip events and subsequent recrystallization under frictionally heated conditions. This is discussed further below in section 7.

There is a subtle effect of grain size on the recorded temperatures. The fine-grained gouges (DET-g) show a larger variation in temperatures than the coarser breccias (DET-b), with the gouges recording more extreme temperatures at both the cold and hot ends of the spectrum. The hottest gouge samples measured here are

>200 °C, while the hottest breccia is only 153 °C. At the cold end, gouges recorded temperatures down to 3 °C, while breccias recorded temperatures down to 20 °C. The 3–15 °C temperatures, which may represent the effect of late, near-surface meteoric fluids on the fault, are only found in the finest texture samples, where the small grain sizes are more susceptible to recrystallization.

6. Heart Mountain Detachment (HMD)

6.1. HMD Geologic Background

The Heart Mountain detachment is a low-angle slip surface with apparent slip of as much as 45 km, which is currently exposed in a ~70 km by 30 km area (Pierce, 1980; Figure 6). At present, the detachment is subhorizontal (<10° dip), and exposures of the upper plate of the detachment form internally coherent masses that show evidence of variable internal extension (Hauge, 1985, 1990).

The allochthon contains two main components, a thin, cratonic Paleozoic section ranging from Ordovician to Mississippian in age, overlain by Eocene (c. 52–48 Ma) volcanic strata of the Absaroka Volcanic Supergroup and related dikes and small intrusive bodies. The fault initially localized within a narrow stratigraphic interval (<5 m thickness) near the base of the dolomitic Ordovician Bighorn Formation, but because of internal distension of the allochthon, both its Paleozoic and Tertiary components lie along the fault plane (e.g., Hauge, 1985, 1990). The fault lies along the eastern margin of the extensive Absaroka volcanic field and was active during Absaroka magmatism (e.g., Douglas et al., 2003; Feeley & Cosca, 2003; Hiza, 2000; Swanson et al., 2016).

6.2. HMD Isotopic Data

A summary of the isotopic data for the 83 samples from the Heart Mountain detachment can be found in Table 2 and is plotted, keyed by texture, in Figure 7. They are discussed below, first with the host rock, then from footwall to hanging wall. Host rock samples (host) have $\delta^{18}O$ values of 22 to 27‰ and $\delta^{13}C$ values of −2 to 4‰. Apparent temperatures are 48 to 60 °C for the Paleozoic units and 39 °C for a single sample of the Jurassic Sundance Formation. Calculated fluid $\delta^{18}O$ values are −4 to 3‰. These values are consistent with diagenesis shortly after formation, reflecting depths of up to ~1 km, with the Jurassic sample being diagenetically altered at a shallower depth than the Paleozoic rocks.

The only footwall vein (FW-v) collected that was large enough to analyze has a $\delta^{18}O$ value of 22.4‰, a $\delta^{13}C$ value of 0‰, a precipitation temperature of 55 °C, and calculated fluid $\delta^{18}O$ value of −3‰. These values are within the range of Cambrian host values.

Detachment breccias (DET-b) have $\delta^{18}O$ values of 12 to 30‰, $\delta^{13}C$ values of −3 to 4‰, precipitation temperatures of 17 to 75 °C, and calculated fluid $\delta^{18}O$ values of −12 to 7‰. These large ranges are consistent with that expected from mixtures of various proportions of the other materials listed here (e.g., host rock, vein fill material, and gouge). Texturally, these detachment breccias contain clasts that can be identified as host rock, vein fill material, or preexisting gouges. However, the bulk of the material is too fine grained to determine its origin based on appearance.

Marble breccia (DET-m) samples have $\delta^{18}O$ values of 21 to 27‰, $\delta^{13}C$ values of −3 to −2‰, apparent temperatures of 128 to 285 °C, and calculated fluid $\delta^{18}O$ values of 13 to 17‰. These compositions are consistent with conditions present during metamorphic reactions immediately following the intrusion of hot magmatic rocks (e.g., Sharp, 2007). The white color and marble texture of the host in this location supports this interpretation and is not found in or near any of the other samples.

Clastic dikes (HW-c) contain carbonate with $\delta^{18}O$ values of 10 to 25‰, $\delta^{13}C$ values of −2 to 1‰, apparent temperatures of 39 to 85 °C, and calculated fluid $\delta^{18}O$ values of −12 to 4‰. These large ranges reflect the variety of carbonate sources contained within these mixtures.

Hanging wall veins and void fills (HW-v) have $\delta^{18}O$ values of 11 to 22‰, $\delta^{13}C$ values of −4 to 3‰, precipitation temperatures of 19 to 65 °C, and calculated fluid $\delta^{18}O$ values of −13 to −7‰. These values of $\delta^{18}O_{water}$ are indicative of a meteoric water source for these materials, with the temperature variations likely reflecting differences in depth at time of formation.

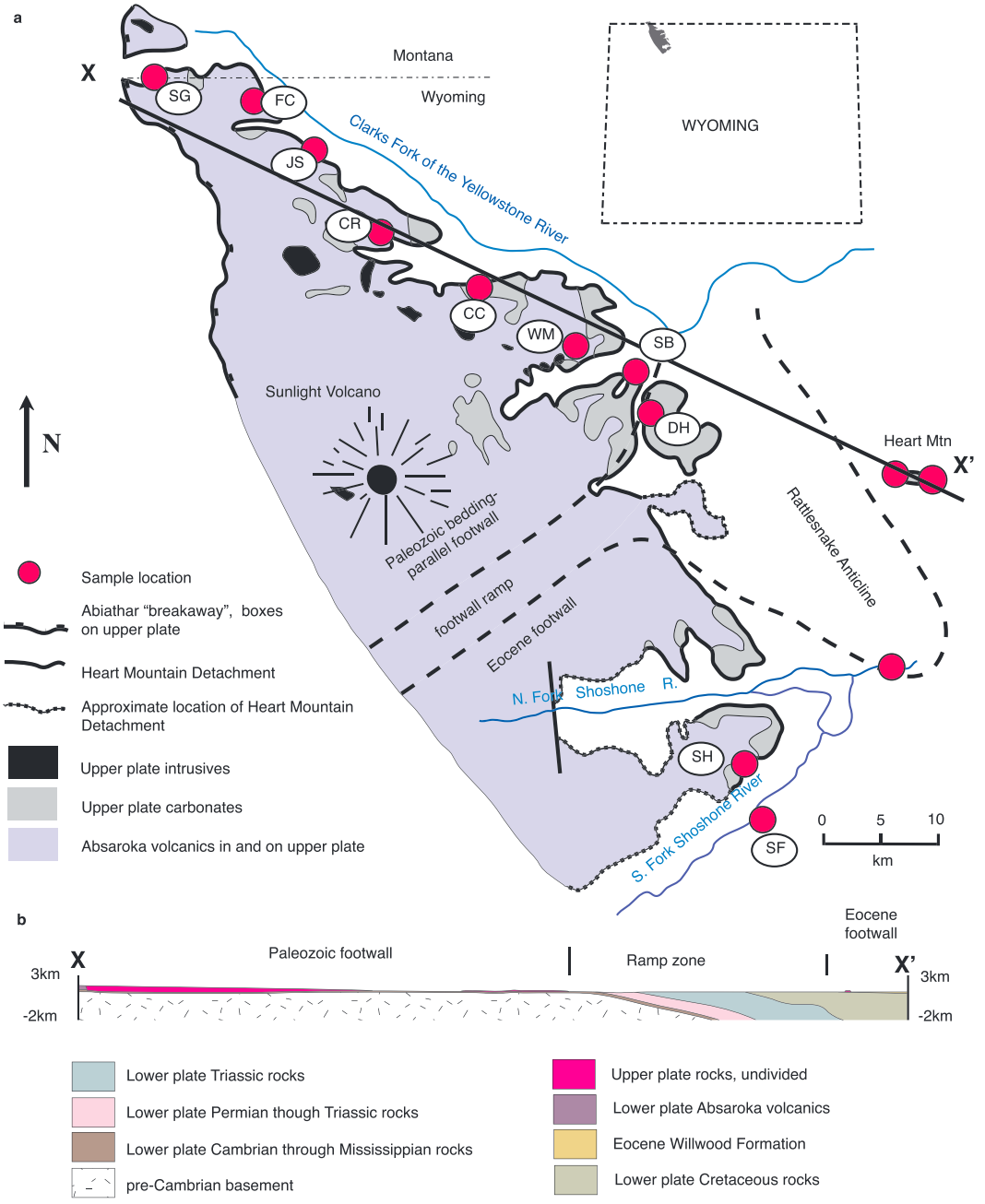

Figure 6. (a) Simplified tectonic map, with inset showing location of study area within Wyoming and (b) 1:1 cross section of the Heart Mountain allochthon. SG, Silvergate; FC, Fox Creek; JS, Jim Smith Creek; CR, Crandall Creek; CC, Cathedral Cliffs; WM, White Mountain; SB, Steamboat; DH, Dead Indian Hill; SH, Sheep Mountain; SF, South Fork of the Shoshone River. Map is modified from Pierce (1980).

Hanging wall fault breccias (HW-f) have $\delta^{18}O$ values of 17 to 26‰, $\delta^{13}C$ values of −3 to 0‰, apparent temperatures of 76 to 573 °C, and calculated fluid $\delta^{18}O$ values of 0 to 19‰. These values, particularly the high temperatures, are unlike any of the source materials, with the exception of the marbles. However, all of these samples are at least 7 km from any source marbles, and there is no evidence of marble texture in any of the samples from these hanging wall faults.

Gouge samples (HW-g) have $\delta^{18}O$ values of 18 to 31‰, $\delta^{13}C$ values of −3 to 4‰, apparent temperatures of 24 to 186 °C, and calculated fluid $\delta^{18}O$ values of −12 to 12‰. These large ranges reflect the variation of materials contained within these mixtures (see Table 3 and discussion below).

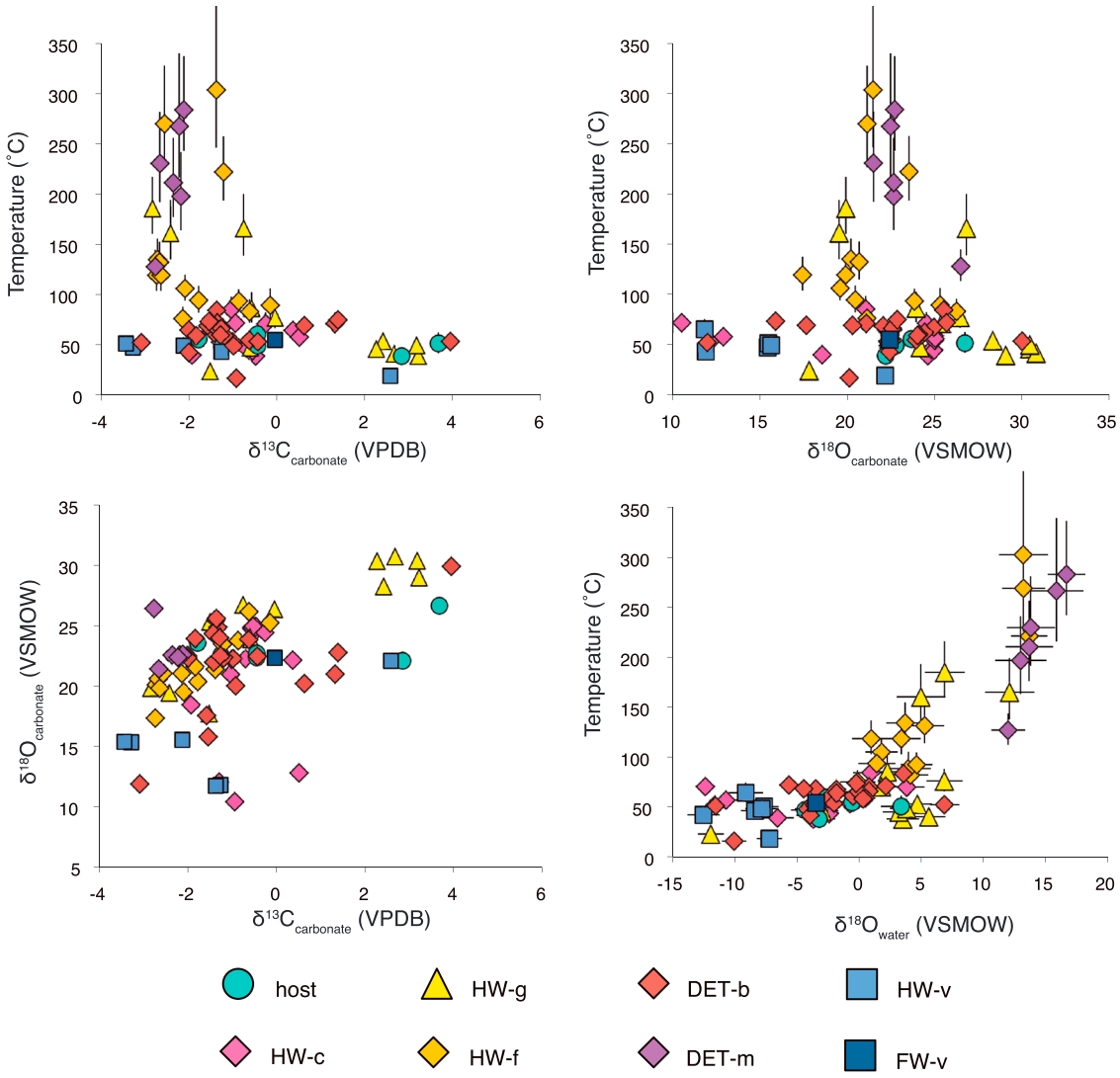

Figure 7. Isotopic data for samples from near the Heart Mountain allochthon, Wyoming, keyed by texture. Errors are 1-sigma standard errors and smaller than the symbol size for $\delta^{18}O_{carbonate}$ and $\delta^{13}C$ analyses. HW, hanging wall; FW, footwall; DET, detachment; g, gouge; b, breccia; v, vein material; m, marble; f, fault; c, clastic dike.

The samples that are mixtures (DET-b, HW-c, HW-f, and HW-g) show carbon and oxygen isotopic compositions of carbonate that could result from mixtures of the host rock, warm vein material, and cold vein material, but the higher temperatures of HW-f, and HW-g require an additional source material that crystallized under hot conditions.

6.3. HMD Discussion

The distribution of temperatures is different from that expected if magmatic fluids or frictional heating were dominant along the Heart Mountain detachment during deformation. While a few samples from the hanging wall yielded high temperatures, the majority of the samples are rather cold (Figure 7). Of the 83 samples, 63 had average crystallization temperatures under 100 °C, a highly counterintuitive finding given that the Heart Mountain detachment essentially accommodates the collapse of an active volcanic center. There is no evidence of hydrothermal fluids or frictional heating along the detachment.

Also enigmatic is the geographic location of the hot samples: while the 6 samples from White Mountain (where the host rock is marble) all record temperatures of at least 125 °C, the remaining 12 samples with temperatures over 100 °C come from hanging wall faults in areas with no volcanic rocks or plutons in the

immediate vicinity and which now lie well away from volcanic centers. With the exception of the marble-hosted samples from White Mountain, not a single sample from within 5 m of the detachment (out of 37 samples) has a temperature over 90 °C.

Elevated temperatures are, however, recorded in hanging wall fault rocks. The two hanging wall faults we sampled are both at low angles to the subhorizontal main detachment, dipping <30°. Both faults preserve a similar, primary texture of Bighorn Formation in their footwalls and brecciated Bighorn Formation in their hanging walls. They lie toward the "toe or runout" area of the Heart Mountain allochthon. The Steamboat site lies at the bottom of the "footwall ramp", where the detachment cuts upsection (and uphill in modern topography) eastward toward the Bighorn Basin. Heart Mountain lies within the Bighorn Basin itself (Figure 6). The Heart Mountain exposure, in particular, is the most easterly exposure of the detachment. Given this location, the allochthon might be expected to have experienced a degree of horizontal contraction, and as such, we suspect that the low-angle fault in the hanging wall of the detachment there might actually be an excised splay of the original detachment, faulted upward, such that it now resides entirely within the hanging wall.

Possible sources of heat for these hanging wall fault samples are direct contact with volcanic or plutonic rocks (i.e., contact metamorphism), elevated geothermal gradient due to the 1–3 km-thick stack of volcanic rocks above, and frictional heating along the faults during slip. The first possibility is not favored due to the lack of proximal exposures of volcanic rocks and the sedimentary, not metamorphic, textures of these rocks. Regarding the second possibility, there is, if anything, an *anti*correlation between samples recording the hottest temperatures and the inferred thickness of volcanic deposits that may have once lay above them (based on proximity to the volcanic centers), with no volcanic rocks surviving erosion (Figure 6). In contrast, samples from areas that lie beneath kilometer-scale thicknesses of volcanic rocks show temperatures that are barely elevated, on the order of ~10 °C above the host rock temperature. Given this disparity, we prefer the third possibility, where the heat recorded within the hanging wall faults owes its origin to frictional heating during slip. This is supported by the lack of elevated temperatures in the wall rock just outside of these fault breccias and gouges.

We stress again that of all the detachment breccia (DET-b) and clastic dike (HW-c) samples we analyzed ($n = 37$), none are hotter than 90 °C. There are two main possibilities for this observation: either samples were cold during fault slip or samples got hot during slip, but the heating signal was not preserved. Preservation of a heating signal would not occur if (1) carbonate minerals did not recrystallize under hot conditions, (2) the hot material later recrystallized under cold conditions, (3) the hot material was later removed via tectonics or dissolution, or (4) the hot carbonate was overwhelmed by volumetrically more significant cold material. We prefer the interpretation that heating occurred but was overprinted, due to the preservation of the shear heating signal at Heart Mountain and the widespread occurrence of meteoric signatures in these colder samples. In the case of the Heart Mountain samples, it is clear that this fault experienced many episodes of slip, with gouge overprinting earlier brecciation and veining events, in turn incorporated as clasts in later breccias (Swanson et al., 2016). Additionally, a void fill sample along the detachment that overprints brecciation gives relatively warm temperatures of 47 and 51 °C, which precludes its formation as a late-stage, near-surface cavity fill. It may have formed during rapid cooling immediately after slip or at a much later time while the fault zone was still at 1 to 2-km depth, depending on the local geothermal gradient.

7. Comparison of the Mormon Peak and Heart Mountain Detachments

The distributions of stable and clumped isotopic compositions show broadly similar trends for both the Mormon Peak and Heart Mountain detachments (Figure 8). The majority of samples have compositions that can be explained by mixtures of host rock, veins, and a higher-temperature material. In fine-grained breccias or gouges, it can be difficult to distinguish these materials without the temperature information from clumped-isotope thermometry. In regard to the plot of $\delta^{18}O_{water}$ versus temperature, the distinctive concave-up shape and broad range of fluid isotopic compositions of the data array (>30‰) reflect the buffering of the fluid composition by the rocks they are in equilibrium with. A summary of the different characteristics of each of these materials can be found in Table 3, and a schematic representation of the large-scale similarities and differences between the two detachment systems is depicted in Figure 9.

Aside from the marble-hosted rocks at White Mountain, the highest temperatures recorded reached more than 200 °C for both areas, with textural relationships consistent with frictional heating. Both areas also

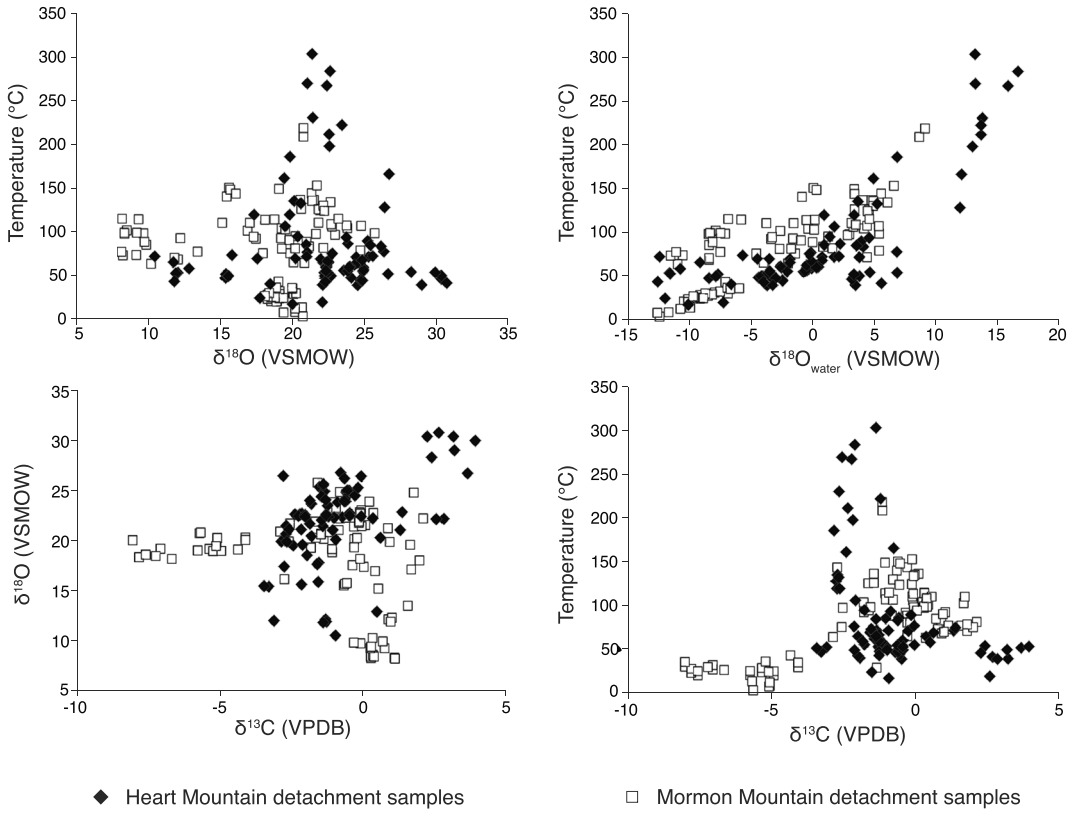

Figure 8. Isotopic data, keyed by detachment fault area.

show isotopic evidence for the predominant source of water along the fault being meteoric, particularly within the vein and void fill samples. Despite proximity to volcanic centers, there is little evidence in either area for precipitation of carbonate from any magma-derived fluids.

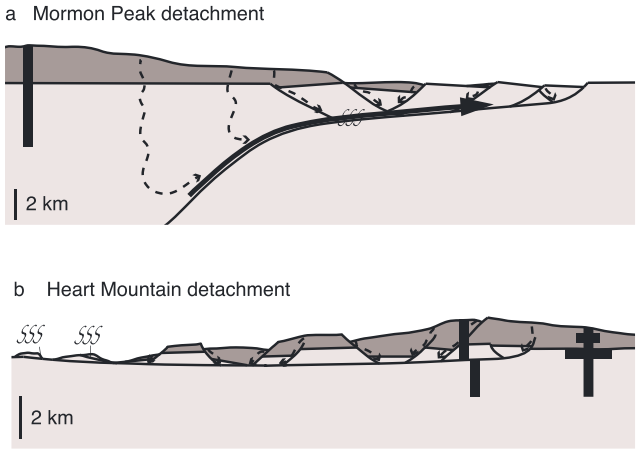

Figure 9. Schematic diagram summarizing comparison between (a) Mormon Peak and (b) Heart Mountain isotopic results. Dashed, wavy lines with arrows, infiltration of meteoric water; solid line with arrow, updip migration of meteoric fluid; "s" pattern, shear heating on detachment and hanging wall faults; heavy vertical and horizontal lines, volcanic source regions; dark gray, Tertiary volcanics; light gray, Precambrian/Paleozoic substrate.

A major difference between the two study areas is the paleodepths sampled by the fault rocks (Figure 9). The Mormon Peak detachment has rocks in its footwall that were at depths of as much as c. 6 km during slip. In contrast, the Heart Mountain allochthon, being rootless, never reached depths of greater than 2 km. This difference is reflected in the temperatures of the warmest veins (and thereby the warmest fluids), with the warmest vein at Heart Mountain recording a temperature of 65 °C, much colder than the vein temperatures associated with the Mormon Peak detachment, which reach up to 115 °C in the hanging wall, and 165 °C in the footwall. Thus, while these two detachments are similar in many aspects, including textures (e.g., Anders et al., 2006), there is a distinct difference in tectonic context.

Samples from the Mormon Mountains are generally warmer than their textural equivalents in the Heart Mountain area (Figure 8). This would not be expected if magmatic processes were intimately related to slip processes along the fault, because the Mormon Mountains are significantly farther from magmatic centers. Instead, the ambient temperatures owing to paleodepth seem to play a dominant role.

Sample temperatures that do not appear to be controlled by ambient conditions (or host rock diagenesis) include the hottest samples. These samples are fine-grained gouges and breccias along slip surfaces, and we interpret them to have been frictionally heated. The gouge

samples that preserve hot temperatures were collected from two localities within the Heart Mountain area and one locality from the Mormon Mountains. The preservation of the heating signal appears to be better along hanging wall faults, which were not sampled in the Mormon Mountains. There is a possibility that the hot samples from the Mormon Mountains were originally on a hanging wall fault that was faulted down onto the detachment surface, but it is more likely that these samples were heated while on the detachment.

Other workers have discussed evidence for decarbonation reactions along the HMD slip surface and elsewhere (Collettini et al., 2013; Mitchell et al., 2015; Rowe et al., 2012). However, we cannot, from isotopic data alone, either strengthen or weaken that argument, as the observed changes in Δ_{47} are explained equally well by heating without decarbonation. But if decarbonation causes fractionation in the O and/or C isotopes, we do not see such changes, as the hotter samples are indistinguishable from the host rock in $\delta^{18}O$ and $\delta^{13}C$.

Given that some hanging wall faults do preserve this heating signal, the hot carbonate may have existed while the detachment was at depth but was overprinted by further, colder fluid infiltration or further slip events. It is also plausible that displacement on the detachment occurred solely by aseismic creep and was therefore not heated frictionally, while seismic slip occurred on the hanging wall faults, a possible explanation for geodetic and seismic data from the Alto Tiberina fault in central Italy, an active low-angle normal fault (e.g., Hreinsdóttir & Bennett, 2009). But given the more depleted $\delta^{18}O_{water}$ isotopic compositions on the main detachment surface, we think that it is more likely that the main fault was more thoroughly overprinted by late-stage, meteoric water infiltration than hanging wall faults.

The better preservation of hot samples along hanging wall faults could arise from the more protracted slip history (and more frequent permeability-increasing events) on the main detachment than on any given hanging wall splay. Continuing slip events probably continue to break new rock and enhance permeability with each event. In contrast, hanging wall faults may experience a much more limited history of slip and may seal over time, resulting in "isolation" from fluid flow along the detachment. It seems likely that with continued slip and permeability enhancement, authigenic carbonate precipitated from meteoric water comprises an increasing proportion of the carbonate in fault zone rocks late in the history of movement.

Aseismic creep and frictional heating from seismic slip are not mutually exclusive processes, and both may have occurred. Indeed, we prefer such an interpretation for the main low-angle detachments, because aseismic pressure solution creep provides a mechanism to locally rotate the stress field, without which rapid slip events could not occur along the low angle slip surface (Swanson et al., 2016).

8. Conclusions

Carbonate clumped-isotope ratios are capable of recording the transient elevation of temperatures from frictional heating along detachments, although preservation of the elevated temperatures along the main detachment surfaces is not common, based on our limited survey. It appears that hanging wall faults related to slip on these surfaces, or fragments of the detachment incorporated into the allochthons, better preserved the record of frictional heating. These data could support the hypothesis of greater heating occurring on the hanging wall faults relative to the main detachment, but given the large fraction of samples with colder meteoric water signatures, the effects of overprinting and sample preservation seem to be more dominant.

Magmatic processes appear to play a very minor role, if any, in the carbonate isotopic signature along either the Mormon Peak or Heart Mountain detachments, except in the White Mountain area. This result is contrary to the suggestion of a number of authors (e.g., Aharonov & Anders, 2006; Anderson et al., 2010; Diehl et al., 2010; Hughes, 1970; Parsons & Thompson, 1993) that magmatic fluids play a significant role in the evolution of detachments.

There is, however, plentiful evidence for meteoric fluids along these detachments. The majority of fault zone material is depleted in $\delta^{18}O$ and cold relative to the host rock, indicating the addition of material that precipitated from meteoric water. This supports various hypotheses for slip along these detachments that involve meteoric fluids, possibly including creep from dissolution and reprecipitation, as suggested by Swanson et al. (2016). The abundance of cold material in the majority of samples appear to reflect significant precipitation from meteoric fluids migrating along the faults.

Acknowledgments

We are indebted to two anonymous reviewers for comments that contributed substantially to the clarity of presentation. This research was supported by National Science Foundation grant EAR 12-50565 awarded to B. P. Wernicke and J. Eiler and by the Caltech Tectonics Observatory of the Gordon and Betty Moore Foundation. Data presented and discussed here are all in the tables and supporting information presented with this manuscript.

References

Aharonov, E., & Anders, M. H. (2006). Hot water: A solution to the Heart Mountain detachment problem? *Geology*, *34*(3), 165.

Anders, M. H., Christie-Blick, N., & Walker, C. D. (2006). Distinguishing between rooted and rootless detachments: A case study from the Mormon Mountains of southeastern Nevada. *Journal of Geology*, *114*(6), 645–664.

Anders, M. H., Fouke, B. W., Zerkle, A. L., Tavarnelli, E., Alvarez, W., & Harlow, G. E. (2010). The role of calcining and basal fluidization in the long runout of carbonate slides: An example from the Heart Mountain slide block, Wyoming and Montana, U.S.A. *The Journal of Geology*, *118*(6), 577–599. https://doi.org/10.1086/656383

Anderson, R. E., Felger, T. J., Diehl, S. F., Page, W. R., & Workman, J. B. (2010). Integration of tectonic, sedimentary and geohydrological processes leading to small-scale extension model for the Mormon Mountains area north of Lake Mead, Lincoln County, Nevada. In P. J. Umhoefer, L. S. Beard, & M. A. Lamb (Eds.), *Miocene tectonics of the Lake Mead Region, Central Basin and Range*, *Geological Society of America Special Paper* (Vol. 463, pp. 395–426).

Axen, G. J. (1992). Pore pressure, stress increase, and fault weakening in low-angle normal faulting. *Journal of Geophysical Research*, *97*(B6), 8979–8992.

Axen, G. J. (2004). Mechanics of low-angle normal faults. In G. D. Karner, B. Taylor, N. W. Driscoll, & D. L. Kohlstedt (Eds.), *Rheology and deformation of the lithosphere at continental margins* (pp. 46–91). New York: Columbia University Press.

Axen, G. J., Wernicke, B. P., Skelly, M. F., & Taylor, W. J. (1990). Mesozoic and Cenozoic tectonics of the Sevier thrust belt in the Virgin River valley area, southern Nevada Basin and Range extensional tectonics near the latitude of Las Vegas, Nevada. *Geological Society of America Memoirs*, *176*, 123–153.

Bergmann, K. D. (2013). *Constraints on the carbon cycle and climate during the early evolution of animals* (PhD dissertation). Pasadena, CA: California Institute of Technology.

Beutner, E. C., & Hauge, T. A. (2009). Heart Mountain and South Fork fault systems: Architecture and evolution of the collapse of an Eocene volcanic system, northwest Wyoming. *Rocky Mountain Geology*, *44*(2), 147–164.

Bidgoli, T. S., Stockli, D. F., & Walker, J. D. (2015). Low-temperature thermochronologic constraints on the kinematic histories of the Castle Cliffs, Tule Springs, and Mormon Peak detachments, southwestern Utah and southeastern Nevada. *Geosphere*, *11*(3), 850–867. https://doi.org/10.1130/GES01083.1

Bonifacie, M., Calmels, D., & Eiler, J. (2013). Clumped isotope thermometry of marbles as an indicator of the closure temperatures of calcite and dolomite with respect to solid-state reordering of C–O bonds. *Mineralogical Magazine*, *77*(5), 735.

Bonifacie, M., Ferry, J. M., Horita, J., Vasconcelos, C., Passey, B. H., & Eiler, J. M. (2011). Calibration and applications of the dolomite clumped isotope thermometer to high temperatures. *Mineralogical Magazine*, *75*(3), 551.

Bos, B., & Spiers, C. J. (2001). Experimental investigation into the microstructural and mechanical evolution of phyllosilicate-bearing fault rock under conditions favouring pressure solution. *Journal of Structural Geology*, *23*, 1187–1202.

Collettini, C., Viti, C., Tesei, T., & Mollo, S. (2013). Thermal decomposition along natural carbonate faults during earthquakes. *Geology*, *41*(8), 927–930. https://doi.org/10.1130/G34421.1

Collettini, C., & Holdsworth, R. E. (2004). Fault zone weakening and character of slip along low-angle normal faults: Insights from the Zuccale fault, Elba, Italy. *Journal of the Geological Society of London*, *161*, 1039–1052.

Cowan, D. S. (1999). Do faults preserve a record of seismic slip? A field geologist's opinion. *Journal of Structural Geology*, *21*, 995–1001.

De Paola, N., Chiodini, G., Hirose, T., Cardellini, C., Caliro, S., & Shimamoto, T. (2011). The geochemical signature caused by earthquake propagation in carbonate-hosted faults. *Earth and Planetary Science Letters*, *310*(3–4), 225–232. https://doi.org/10.1016/j.epsl.2011.09.001

Defliese, W. F., & Lohmann, K. C. (2015). Non-linear mixing effects on mass-47 CO_2 clumped isotope thermometry: Patterns and implications. *Rapid Communications in Mass Spectrometry*, *29*(9), 901–909. https://doi.org/10.1002/rcm.7175

Dennis, K. J., Affek, H. P., Passey, B. H., Schrag, D. P., & Eiler, J. M. (2011). Defining an absolute reference frame for 'clumped' isotope studies of CO_2. *Geochimica et Cosmochimica Acta*, *75*(22), 7117–7131. https://doi.org/10.1016/j.gca.2011.09.025

Diehl, S. F., Anderson, R. E., & Humprey, J. D. (2010). Fluid flow, solution collapse, and massive dissolution at detachment faults, Mormon Mountains, Nevada. In P. J. Umhoefer, L. S. Beard, & M. A. Lamb (Eds.), *Miocene tectonics of the Lake Mead Region, Central Basin and Range*, *Geological Society of America Special Paper* (Vol. 463, pp. 427–441). https://doi.org/10.1130/2010.2463(19)

Douglas, T. A., Chamberlain, C. P., Poage, M. A., Abruzzese, M., Schultz, S., Henneberry, J., & Layer, P. (2003). Fluid flow and the Heart Mountain fault: A stable isotopic, fluid inclusion, and geochronologic study. *Geofluids*, *3*, 13–32.

Eiler, J. M. (2007). "Clumped-isotope" geochemistry—The study of naturally-occurring, multiply-substituted isotopologues. *Earth and Planetary Science Letters*, *262*(3-4), 309–327. https://doi.org/10.1016/j.epsl.2007.08.020

Eiler, J. M. (2011). Paleoclimate reconstruction using carbonate clumped isotope thermometry. *Quaternary Science Reviews*, *30*(25–26), 3575–3588. https://doi.org/10.1016/j.quascirev.2011.09.001

Feeley, T. C., & Cosca, M. A. (2003). Time vs. composition trends of magmatism at Sunlight volcano, Absaroka volcanic province, Wyoming. *Geological Society of America Bulletin*, *115*(6), 714–728.

Forsyth, D. W. (1992). Finite extension and low-angle normal faulting. *Geology*, *20*(1), 27–30. https://doi.org/10.1130/0091-7613(1992)020<0027:FEALAN>2.3.CO;2

Guo, W. F., Mosenfelder, J. L., Goddard, W. A. III, & Eiler, J. M. (2009). Isotopic fractionations associated with phosphoric acid digestion of carbonate minerals: Insights from first-principles theoretical modeling and clumped isotope measurements. *Geochimica et Cosmochimica Acta*, *73*(24), 7203–7225.

Han, R., Hirose, T., & Shimamoto, T. (2010). Strong velocity weakening and powder lubrication of simulated carbonate faults at seismic slip rates. *Journal of Geophysical Research*, *115*, B03412. https://doi.org/10.1029/2008JB006136

Hauge, T. A. (1985). Gravity-spreading origin of the Heart Mountain allochthon, northwestern Wyoming. *Geological Society of America Bulletin*, *96*(11), 1440–1456. https://doi.org/10.1130/0016-7606(1985)96<1440:GOOTHM>2.0.CO;2

Hauge, T. A. (1990). Kinematic model of a continuous Heart Mountain allochthon. *Geological Society of America*, *102*(9), 1,174–1,188. https://doi.org/10.1130/0016-7606(1990)102<1174:KMOACH>2.3.CO;2

Henkes, G. A., Passey, B. H., Grossman, E. L., Shenton, B. J., Pérez-Huerta, A., & Yancey, T. E. (2014). Temperature limits for preservation of primary calcite clumped isotope paleotemperatures. *Geochimica et Cosmochimica Acta*, *139*, 362–382. https://doi.org/10.1016/j.gca.2014.04.040

Hickman, S., & Zoback, M. (2004). Stress orientations and magnitudes in the SAFOD pilot hole. *Geophysical Research Letters*, *31*, L15S12. https://doi.org/10.1029/2004GL020043

Hirose, T., & Shimamoto, T. (2005). Growth of a molten zone as a mechanism of slip weakening of simulated faults in gabbro during frictional melting. *Journal of Geophysical Research*, *110*, B05202. https://doi.org/10.1029/2004JB003207

Hiza, M. M. (2000). The geochemistry and geochronology of the Eocene Absaroka Volcanic Province, Northern Wyoming and Southwest Montana, USA [Doctor of Philosophy: Oregon State University, 240 p.
Hreinsdóttir, S., & Bennett, R. A. (2009). Active aseismic creep on the Alto Tiberina low-angle normal fault, Italy. *Geology*, *37*(8), 683–686. https://doi.org/10.1130/G30194A.1
Hughes, C. J. (1970). The Heart Mountain detachment fault: A volcanic phenomenon? *Journal of Geology*, *78*, 107–116.
Huntington, K. W., Eiler, J. M., Affek, H. P., Guo, W., Bonifacie, M., Yeung, L. Y., et al. (2009). Methods and limitations of "clumped" CO_2 isotope (Δ47) analysis by gas-source isotope ratio mass spectrometry. *Journal of Mass Spectrometry*, *44*(9), 1318–1329.
Lister, G. S., & Baldwin, S. L. (1993). Plutonism and the origin of metamorphic core complexes. *Geology*, *21*(7), 607–610. https://doi.org/10.1130/0091-7613(1993)021<0607:PATOOM>2.3.CO;2
Lister, G. S., & Davis, G. A. (1989). The origin of metamorphic core complexes and detachment faults formed during Tertiary continental extension in the northern Colorado River region, U.S.A. *Journal of Structural Geology*, *11*, 65–94.
Livaccari, R. F., & Geissman, J. W. (2001). Large-magnitude extension along metamorphic core complexes of western Arizona and southeastern California: Evaluation with paleomagnetism. *Tectonics*, *20*(5), 625–648.
Lockner, D. A., Morrow, C., Moore, D., & Hickman, S. (2011). Low strength of deep San Andreas fault gouge from SAFOD core. *Nature*, *472*(7341), 82–85.
Losh, S. (1997). Stable isotope and modeling studies of fluid-rock interaction associated with the Snake Range and Mormon Peak detachment faults, Nevada. *Geological Society of America Bulletin*, *109*(3), 300–323.
Melosh, H. J. (1990). Mechanical basis for low-angle normal faulting in the Basin and Range province. *Nature*, *343*(6256), 331–335. https://doi.org/10.1038/343331a0
Mitchell, T. M., Smith, S. A., Anders, M. H., Di Toro, G., Nielsen, S., Cavallo, A., & Beard, A. D. (2015). Catastrophic emplacement of giant landslides aided by thermal decomposition: Heart Mountain, Wyoming. *Earth and Planetary Science Letters*, *411*, 199–207. https://doi.org/10.1016/j.epsl.2014.10.051
Morley, C. K. (2014). The widespread occurrence of low-angle normal faults in a rift setting: Review of examples from Thailand, and implications for their origin and evolution. *Earth-Science Reviews*, *133*, 18–42.
Mount, V. S., & Suppe, J. (1987). State of stress near the San Andreas fault: Implications for wrench tectonics. *Geology*, *15*(12), 1143–1146.
O'Neil, J. R., Clayton, R. N., & Mayeda, T. K. (1969). Oxygen isotope fractionation in divalent metal carbonates. *Journal of Chemical Physics*, *51*(12), 5547–5558. https://doi.org/10.1063/1.1671982
Parsons, T., & Thompson, G. A. (1993). Does magmatism influence low-angle normal faulting? *Geology*, *21*(3), 247–250. https://doi.org/10.1130/0091-7613(1993)021<0247:DMILAN>2.3.CO;2
Passey, B. H., & Henkes, G. A. (2012). Carbonate clumped isotope bond reordering and geospeedometry. *Earth and Planetary Science Letters*, *351*, 223–236.
Pierce, W. G. (1980). The Heart Mountain break-away fault, northwestern Wyoming. *Geological Society of America Bulletin*, *91*(5), 272–281. https://doi.org/10.1130/0016-7606(1980)91<272:THMBFN>2.0.CO;2
Rice, J. R. (1992). Chapter 20: Fault stress states, pore pressure distributions, and the weakness of the San Andreas Fault. In E. Brian & W. Teng-fong (Eds.), *International Geophysics* (Vol. 51, pp. 475–503). Academic Press. Retrieved from https://www.sciencedirect.com/science/article/pii/S0074614208628351
Rice, J. R. (2006). Heating and weakening of faults during earthquake slip. *Journal of Geophysical Research*, *111*, B05311. https://doi.org/10.1029/2005JB004006
Rosenbaum, J., & Sheppard, S. M. F. (1986). An isotopic study of siderites, dolomites and ankerites at high temperatures. *Geochimica et Cosmochimica Acta*, *50*(6), 1147–1150. https://doi.org/10.1016/0016-7037(86)90396-0
Rowe, C. D., Fagereng, Å., Miller, J. A., & Mapani, B. (2012). Signature of coseismic decarbonation in dolomitic fault rocks of the Naukluft Thrust, Namibia. *Earth and Planetary Science Letters*, *333*, 200–210.
Schauble, E. A., Ghosh, P., & Eiler, J. M. (2006). Preferential formation of ^{13}C-^{18}O bonds in carbonate minerals, estimated using first-principles lattice dynamics. *Geochimica et Cosmochimica Acta*, *70*(10), 2510–2529. https://doi.org/10.1016/j.gca.2006.02.011
Scott, R. B., Unruh, D. M., Snee, L. W., Harding, A. E., Nealey, L. D., Blank, H. R., et al. (1995). Relation of peralkaline magmatism to heterogeneous extension during the middle Miocene, southeastern Nevada. *Journal of Geophysical Research*, *100*(B6), 10,381–10,401.
Scott, R. J., & Lister, G. S. (1992). Detachment faults: Evidence for a low-angle origin. *Geology*, *20*(9), 833–836.
Sharp, Z. D. (2007). *Principles of stable isotope geochemistry*. Upper Saddle River, NJ: Pearson Prentice Hall.
Sibson, R. H. (1975). Generation of pseudotachylyte by ancient seismic faulting. *Geophysical Journal of the Royal Astronomical Society*, *43*, 775–794.
Sibson, R. H. (1977). Fault rocks and fault mechanisms. *Journal of the Geological Society of London*, *133*(3), 191–213. https://doi.org/10.1144/gsjgs.133.3.0191
Smedes, H. W., & Prostka, H. J. (1972). Stratigraphic framework of the Absaroka Volcanic Supergroup in the Yellowstone National Park region: U.S. Geological Survey Professional Paper, v. 729-C, p. 1–33.
Snoke, A. W., Tullis, J., & Todd, V. R. (1998). *Fault-related rocks. A photographic atlas* (p. 617). Princeton, NJ: Princeton Univ. Press.
Stolper, D. A., & Eiler, J. M. (2015). The kinetics Of solid-state isotope-exchange reactions for clumped isotopes: A study of inorganic calcites and apatites from natural and experimental samples. *American Journal of Science*, *315*(5), 363–411. https://doi.org/10.2475/05.2015.01
Sulem, J., & Famin, V. (2009). Thermal decomposition of carbonates in fault zones: Slip-weakening and temperature-limiting effects. *Journal of Geophysical Research*, *114*, B03309. https://doi.org/10.1029/2008JB006004
Swanson, E., & Wernicke, B. (2017). Geologic map of the east-central Meadow Valley Mountains, and implications for reconstruction of the Mormon Peak detachment, Nevada. *Geosphere*, GES01148.01141.
Swanson, E., Wernicke, B. P., & Hauge, T. A. (2016). Episodic dissolution, precipitation, and slip along the Heart Mountain detachment, Wyoming. *The Journal of Geology*, *124*(1), 75–97.
Swanson, E. M., Wernicke, B. P., Eiler, J. M., & Losh, S. (2012). Temperatures and fluids on faults based on carbonate clumped-isotope thermometry. *American Journal of Science*, *312*(1), 1–21. https://doi.org/10.2475/01.2012.01
Templeton, A. S., Sweeney, J. J., Manske, H., Tilghman, J. F., Calhoun, S. C., Violich, A., & Chamberlain, C. P. (1995). Fluids and the Heart Mountain fault revisited. *Geology*, *23*(10), 929–932.
Vasconcelos, C., McKenzie, J. A., Warthmann, R., & Bernasconi, S. M. (2005). Calibration of the $\delta^{18}O$ paleothermometer for dolomite precipitated in microbial cultures and natural environments. *Geology*, *33*(4), 317–320. https://doi.org/10.1130/G20992.1
Walker, C. D., Anders, M. H., & Christie-Blick, N. (2007). Kinematic evidence for downdip movement on the Mormon Peak detachment. *Geology*, *35*(3), 259.
Wernicke, B. (1995). Low-angle normal faults and seismicity: A review. *Journal of Geophysical Research*, *100*(B10), 20,159.

Wernicke, B., Walker, J. D., & Beaufait, M. S. (1985). Structural discordance between Neogene detachments and frontal Sevier thrusts, Central Mormon Mountains, Southern Nevada. *Tectonics*, *4*(2), 213–246.

Yin, A. (1989). Origin of regional, rooted low-angle normal faults—A mechanical model and its tectonic implications. *Tectonics*, *8*(3), 469–482.

Zoback, M. D., & Townend, J. (2001). Implications of hydrostatic pore pressures and high crustal strength for the deformation of intraplate lithosphere. *Tectonophysics*, *336*(1–4), 19–30.